EIGHTH EUROPEAN ROTORCRAFT FORUM

Paper No. 3.2

FORMULATION AND SOLUTION OF ROTARY-WING AEROELASTIC STABILITY AND RESPONSE PROBLEMS

Peretz P. Friedmann
Mechanics and Structures Department
University of California at Los Angeles
Los Angeles, California, 90024, U.S.A.

August 31 through September 3, 1982
Aix-En-Provence, France

ASSOCIATION AERONAUTIQUE ET ASTRONAUTIQUE DE FRANCE

FORMULATION AND SOLUTION OF ROTARY-WING AEROELASTIC STABILITY AND RESPONSE PROBLEMS*

Peretz P. Friedmann, Professor
Mechanics and Structures Department
University of California
Los Angeles, California 90024 U.S.A.

ABSTRACT

The state of the art in the formulation and solution of rotary-wing aeroelastic stability and response problems is reviewed in detail. The approximations used in the structural, inertia and aerodynamic operators are discussed. The important role of geometric nonlinearities, due to moderate deflections, and aerodynamic stall in the aeroelastic stability and response problem are identified. It is also shown that geometric nonlinearities are of primary importance in aeroelastic stability calculations, and have a more limited, though important, role in response calculations. Next, formulation of coupled rotor/fuselage problems is described, for both air and ground resonance type problems. Both topics, the isolated blade problem and the coupled rotor/fuselage problem, are treated for both hover and forward flight. Solution of aeroelastic stability and response problems proceed in two stages. First, the spatial dependence is eliminated by using Galerkin's method, or by using the finite element method. Next the nonlinear, or linear, ordinary differential equation with periodic coefficients have to be solved for stability or response. Efficient numerical methods for accomplishing these objectives are presented in a comprehensive manner. The paper contains a number of illustrative numerical results which are intended to clarify various aspects of the modeling process and serve as representative results for both aeroelastic stability and response calculations for a variety of blade and rotor configurations.

1. Introduction and Objectives

During the last five years which have elapsed since the last review paper on rotary-wing aeroelasticity has been published[1] the literature in the field of rotary-wing unsteady aerodynamics, dynamics and aeroelasticity has increased substantially. In addition to numerous papers dealing with this subject, which will be mentioned when applicable in the paper, it should be also noted that a number of recent books, dealing with these topics, are now available. Of these most notable are, Bramwell's[2] book which contains considerable amount of material on aerodynamics and dynamics, Dowell et al's[3] book on aeroelasticity which contains an introductory chapter dealing with simple and elementary aeroelastic problems in hover, and Johnson's[4] monumental treatise on helicopter theory, which contains extensive, detailed and useful material on aerodynamic, dynamic and mathematical aspects of rotary-wing aerodynamics, dynamics and aeroelasticity.

The new body of literature available on analytical and methodological aspects of rotary-wing dynamic and aeroelastic problems has also been augmented by significant developments in hardware. New concepts such as the ABC rotor[5,6] and the XV-15[7] tiltrotor have been proven in numerous flight tests. The circulation

*This work was supported by the Structures Laboratory AVRADCOM and NASA Langley Research Center under NASA Grant NSG 1578.

controlled rotor[8] and the X-wing[9] have been demonstrated in wind tunnel tests. Bearingless main rotors[10-12] and tail rotors[13-15] have been developed and tested in both wind tunnel and flight tests. New hingeless rotors have been developed as potential replacements for existing teetering rotor systems[16,17]. New articulated rotor systems, representing substantial innovation compared to existing convential types have emerged[18], and the extensive use of composite materials in blade and hub construction is being used by the various helicopter manufacturers[10,11,13-15,19,20].

The developments in hardware, mentioned above, have been accompanied by parallel developments in analytical methods and software which facilitate, analysis, design and simulation involving complex aeroelastic phenomena. Typical of such comprehensive helicopter analysis programs is one which has been recently described by Johnson[21,22]. Even more comprehensive programs such as the Second Generation Comprehensive Helicopter Analysis Program are currently under development, by the U.S. Army and NASA[23].

This substantial body of material which has recently become available is indicative of the fact that rotary-wing aeroelasticity is achieving a degree of maturity which has been somewhat lacking in the past. Methods for formulating and solving rotary-wing aeroelastic stability and response problems have crystalized and are now relatively well established. It is the general objective of this paper to present these methods in some detail and comment on their relative merits, flexibility, limitations and accuracy. Specifically the objectives of the paper are:

(a) To present the state of the art as applicable to the formulation and solution of rotary-wing aeroelastic stability and response problems.
(b) Review some approximations frequently used for deriving the structural, inertia and aerodynamic operators associated with the rotary-wing aeroelastic problem.
(c) Identify the role of nonlinearities, both geometrical and aerodynamic.
(d) Discuss the mathematical techniques used for solving both aeroelastic stability and response problems.
(e) Present some illustrative results and examples.

The presentation of this material will be divided in two parts; namely isolated blade analyses and coupled rotor/fuselage analyses. For each case the modeling of the structural, inertia and aerodynamic component of the aeroelastic problem will be discussed and subsequently the methods available for solving the resulting equations of dynamic equilibrium will be considered in detail.

The methods discussed in the paper are general and valid for most rotary-wing aeroelastic problems, however the examples illustrating the implementation of these methods will be restricted to hingeless or bearingless rotors, mainly because some of the more recent work has been done on these particular configurations.

Finally, it should be clear that when discussing rotary wing aeroelastic problems one should distinguish between three levels, which represent a gradual increase in the degree of complexity. For stability problems one encounters:

- isolated blade aeroelastic stability, which provides a basic understanding of blade dynamics.

- coupled rotor/fuselage aeromechanical stability which deals with air and ground resonance and is indicative of overall system behavior.

- control-coupled aeroelastic problems, where the aeroelastic system is coupled with a higher harmonic control device or an active flutter suppression system.

As shown in this paper, a considerable body of knowledge exists on the first two classes of problems indicated above. The third category is still in a primitive state and will not be treated in this paper.

The same hierarchy of ascending complexity is also evident when one considers aeroelastic response problems:

- blade loads and response, requires adequate aerodynamic modeling as well as detailed structural modeling to calculate dynamic stresses, shears and moments.

- coupled rotor/fuselage vibration problems require both adequate modeling of the aerodynamic loads, which are the source of the excitation, and a good structural model of the fuselage, this topic in the context of vibration control has been treated in a recent survey[26].

- control-coupled vibration problems in presence of higher harmonic or other active load control and response alleviation devices, have been treated in detail in a recent review[27].

2. Formulation of Rotary-Wing Aeroelastic Problems for the Isolated Blade Case

2.1 General

Rotary wing aeroelastic stability or response problems require three basic ingredients for their formulation, namely: structural modeling (i.e., the structural operator), inertia modeling (i.e., the inertia operator) and aerodynamic modeling (i.e., aerodynamic operator).

The modeling process is one which has to be carefully done, the detail and level of sophistication in the analysis is governed to a considerable extent by the goals of the analysis. If an aeroelastic stability analysis is required, recent research[1,24] has indicated that nonlinearities can have a significant role, particular for hingeless and bearingless rotors. The nonlinearities implied here are geometrical nonlinearities associated with the assumption of small strain and moderate deflections in the representation of blade motion. Clearly, aerodynamic nonlinearities such as static or dynamic stall also play an important role, as will be discussed later, however geometric nonlinearities have a wider implication on the formulation of these problems.

On the other hand in aeroelastic response problems there seems to be an indication that the geometrically nonlinear terms might be somewhat less important[25], however the aerodynamic nonlinearities dominate when substantial dynamic stall effects are present.

The general comments made above, apply to a variety of rotor configurations such as a typical hingeless rotor shown in Figure 1 or a typical bearingless rotor such as shown in Figure 2. They also apply to teetering rotors, such as shown in Figure 3, except that in this case the mechanical coupling which

represents rigid body flapping motion, requires a coupled treatment of this two bladed system[1].

2.2 Structural Modeling

When dealing with the rotor configurations shown in Figures 1-3, an important ingredient in the proper modeling of rotary wing aeroelastic stability problems is the incorporation of geometrical nonlinearities due to the assumption of small strains and moderate deflections. This manifests itself in the mathematical structure of the transformation between the triad of unit vectors defining the undeformed state, of the blade, and the triad of unit vectors associated with the deformed state of the blade.

Using a hingeless rotor blade, as a typical example, the undeformed and deformed blade configuration are shown in Figs. 4-5. Such a transformation, based on the assumption of small strains and finite rotations, for a blade undergoing coupled flap, lag and torsional motion, has the following mathematical form[28,29] (the various symbols used throughout this paper are defined in Appendix A)

$$\begin{Bmatrix} \hat{e}_x' \\ \hat{e}_y' \\ \hat{e}_z' \end{Bmatrix} = \begin{bmatrix} 1 & v_{,x} & w_{,x} \\ -(v_{,x}+\phi w_{,x}) & 1 & \phi \\ -(w_{,x}-\phi v_{,x}) & -(\phi+v_{,x}w_{,x}) & 1 \end{bmatrix} \begin{Bmatrix} \hat{e}_x \\ \hat{e}_y \\ \hat{e}_z \end{Bmatrix} =$$

$$= [S] \begin{Bmatrix} \hat{e}_x \\ \hat{e}_y \\ \hat{e}_z \end{Bmatrix}' \tag{1}$$

The inverse transformation is given by

$$\begin{Bmatrix} \hat{e}_x \\ \hat{e}_y \\ \hat{e}_z \end{Bmatrix} = [S]^T \begin{Bmatrix} \hat{e}_x' \\ \hat{e}_y' \\ \hat{e}_z' \end{Bmatrix} \tag{2}$$

which implies $[S]^T = [S]^{-1}$

Transformations of this type, combined with the Euler-Bernoulli assumption have been frequently used to derive moderate deflection beam theories for rotor dynamics applications[1,24,28-30]. This transformation when used in the derivation of the inertia and aerodynamic operators, associated with the rotary-wing aeroelastic problem, yields numerous relatively small nonlinear terms[24,29]. While some, relatively minor, discrepancies between various formulations exist, as has been carefully pointed out in Ref. 31, the important item to note is that coupled flap-lag-torsional solutions based on these equations are generally in good agreement. These moderate deflection beam theories have been also validated by comparing them to static tests performed in the moderate deflection regime[32,33]. When the geometrically nonlinear terms in these equations are neglected they reduce to the well known Houbolt and Brooks equations[34] which are linear equations. However it should be noted that terms representing added torsional rigidity due to pretwist and coupling due to pretwist, between torsion and axial loads, are still being refined in studies which have become recently available[35-37].

The structural models for rotor blades discussed above are all based on the assumption that the blade is isotropic. Modern helicopter rotor blades are built of composite materials. Such materials are not isotropic therefore in composite blades bending and shear effects can be coupled and warping maybe also present. Furthermore, composite materials enable one to introduce special coupling effects which might be beneficial from a dynamic point of view. When one tries to incorporate fiber composite material properties, in a beam theory, one usually finds that the Euler-Bernoulli assumption, that plane sections remain plane and perpendicular to the deformed elastic axis, is no longer valid. In such cases, more refined beam theories might have to be considered[38,39] to adequately model composite blades. Currently the proper structural modeling of composite blades is still in a relatively primitive stage, although a recent paper by Worndle has made a substantial contribution[40].

The representation of the structural redundancies which exist in the blade root region of modern composite main rotor is another important structural problem which requires more complicated models than those used for conventional hingeless blades[41-46]. Reference 46 is indicative of a convenient model which can be used for such a case. Based on current developments in finite element modeling of rotary-wing aeroelastic problems, which will be discussed later in this paper, it appears that the most convenient model for representation of a bearingless rotor would be one which uses a special finite element model for the root portion of the rotor, combined with a conventional beam type finite element model for the outboard section of the blade.

2.3 Inertia Modeling

Derivation of the inertia loads for the isolated blade case is a relatively simple procedure[1,29]. Using the position vector $\bar{R}$ of a mass point of the deformed blade cross section, one obtains the acceleration vector in the inertial system. From elementary mechanics

$$\bar{a} = \ddot{\bar{R}} + 2\bar{\Omega}x\bar{R} + \underline{\dot{\bar{\Omega}}x\bar{R}} + \bar{\Omega}x(\bar{\Omega}x\bar{R}) \qquad (3)$$

The underlined term in Eq. (3) is usually zero for a rotor blade rotating with a fixed angular speed. Distributed inertia loads are obtained directly from D'Alembert's principle. Similarly distributed inertia torques are obtained from the vector product of inertia loads and the position vector of the mass point in the cross section from the blade elastic axis. This, relatively straight-forward procedure can become algebraically tedious, due to the numerous small terms associated with the geometric nonlinearity[24,29].

Modeling of the structural and inertia aspects of the rotary-wing aeroelastic problem, can be algebraically tedious, however conceptually it offers few significant obstacles. This is reason why the state of the art in modeling these two facets, with the exception noted for composite blades, has attained a satisfactory degree of accuracy and sophistication.

2.4 Aerodynamic Modeling

Modeling of the unsteady aerodynamic loads required for rotary-wing aeroelastic analysis presents major challenges to the analyst. A wide array of assumptions can be made which lead to a variety of models, starting with simple and computationally efficient models and culminating in models which are capable of simulating the more intricate details of the unsteady flow. The more sophisticated unsteady aerodynamic models are sometimes severely limited

by prohibitive computing costs, when incorporated in an aeroelastic analysis. It is important to recognize that the rotary-wing aeroelastic problem is one which represents the stability or response, of a complex structural dynamic system to aerodynamic inputs which are very difficult to model in a precise manner.

When attempting to compare experimental aeroelastic stability boundaries[22,47] or response data[22,48] to computations the evidence available suggests that a substantial portion of the discrepancies observed can be attributed to the assumptions used in the modeling of the aerodynamic loads.

A detailed description of unsteady aerodynamics for rotary wing applications has been presented by Johnson[4]. The objective of this section is to emphasize certain aspects of this topic as applied to rotary-wing aeroelasticity.

2.4.1 Hover

Assuming hover combined with low inflow which is also equivalent to low disc loading, and incompressible flow, results in considerable simplification of the unsteady aerodynamic loads.

The simplest type of unsteady aerodynamics which has been used for this case is Theodorsen's theory[49]. The geometry of airfoil, when performing pitching and plunging motions, which are assumed to be simple harmonic, is shown in Fig. 6. The unsteady lift, with the lift curve slope a, replacing 2π, is given by

$$L_u = \rho_A abC(k)U\left[\frac{dh}{dt} + U\Delta\alpha + (b-x_A)\frac{d\Delta\alpha}{dt}\right] + \frac{1}{2}\rho_A ab^2\left[\frac{d^2h}{dt^2} + U\frac{d\Delta\alpha}{dt} - (x_A - \frac{b}{2})\frac{d^2\Delta\alpha}{dt^2}\right] \quad (4)$$

and a similar expression for the moment.

It is well known that Theodorsen's theory is not valid for rotary wings because the unsteady wake beneath a rotor is quite different from the wake postulated by Theodorsen's theory. Nevertheless, various quasi-steady and unsteady models for the aerodynamic loads based upon this theory have been frequently employed in rotary wing aeroelasticity[50].

Even when wake effects are excluded, C(k) = 1, Theodorsen's theory is still not directly applicable to rotor blades undergoing coupled flap-lag-torsional motion[51], because: (1) in addition to constant velocity of the oncoming flow the blade also experiences a time dependent variation due to lead-lag motion, (2) in addition to harmonic variation in angle of pitch, due to blade dynamics, a constant collective pitch setting is also imposed on the airfoil, (3) the plunge velocity $\frac{d}{dt}(h)$ is not purely harmonic, since it contains a steady component due to a constant inflow through the disc.

The first two effects mentioned above have been incorporated in an approximate modification of Theodorsen's theory due to Greenberg[52], the expression obtained for lift is

$$L = \frac{1}{2}\rho_A ab^2 \left[\frac{d^2h}{dt^2} + (V_o+\Delta V)\frac{d\Delta\alpha}{dt} + (\alpha_o+\Delta\alpha)\frac{d(\Delta V)}{dt} - \right.$$

$$\left. - (x_A - \frac{b}{2})\frac{d^2\Delta\alpha}{dt^2}\right] + \rho_A aVbC(k)\left[\frac{dh}{dt} + \alpha_o\Delta V + V_o\Delta\alpha + \right.$$

$$\left. (b-x_A)\frac{d\Delta\alpha}{dt}\right] + \rho_A aVb\left[\underline{V_o\alpha_o} + \underline{\underline{\Delta\sigma\Delta VC(2k)}}\right] \qquad (5)$$

where $V = V_o + \Delta V$; $\Delta V = \sigma_V V_o e^{i\omega t}$; and α_o = constant pitch setting

The last two terms in this theory represent respectively, the static lift (single underlined) and a nonlinear term in the perturbation quantities (double underlined) which is usually neglected in rotary wing applications of this theory. Greenberg's theroy is approximate because he has neglected the effect of fore and aft excursions of the blade, or the effect of the pulsating flow velocity, relative to the mean velocity, on the wake. An expression similar to Eq. (5) is also provided in Ref. 52 for the unsteady moment. A simple correction to this theory to account for constant inflow has been presented in Ref. 51.

Greenberg's theory has recently enjoyed considerable popularity in rotary-wing aeroelasticity[24,30,51,53,54]. In applying this theory, velocity components, relative to the deformed cross section of the blade have to be identified and used.

In applying this theory to rotary wings, certain liberties were taken with Greenberg's theory which extend beyond the assumptions originally made by Greenberg in developing his theory. Thus for example it is assumed that the circulatory portion of the lift acts perpendicular to the resultant velocity of the flow, while the noncirculatory portion of the lift, associated primarily with apparent mass effects, acts perpendicular to the chord of the blade cross section in its deformed state. This distinction between the two contributions to lift is convenient for rotary-wing applications because it yields somewhat simpler expressions for the aerodynamic loads, however it was not made by Greenberg. It is also frequently assumed that the axis of pitch is at the quarter chord, while Greenberg used the elastic axis as the point about which pitching oscillations occur. Furthermore the rate of pitch experienced by the airfoil is sometimes taken as

$$\dot{\alpha} \tilde{=} \dot{\phi} + \Omega(\beta_p + w_{,x}) \qquad (6)$$

Equation (6) implies a constant rate of pitch, given by $\Omega\beta_p$ which was not postulated by Greenberg. Furthermore, when Eq. (6) is integrated in time to yield $\alpha(t)$, it implies a very large angle of attack which appears to be logically inconsistent.

Refinements of Greenberg's theory have also been developed as part of a potential flow solution which was subsequently combined with a boundary layer model and used to estimate the drag of an oscillating airfoil in a fluctuating free stream[55,56].

A theory similar to Greenberg's is also presented in Section 10.4 of Ref. 4, where the effects of the time varying free stream, due to forward flight alone, on the lift defficiency function are discussed in detail.

Recall that Greenberg's theory is essentially a fixed wing type unsteady aerodynamic theory. When the effect of the unsteady wake beneath rotor is required, Loewy's[57] rotary wing unsteady generalization of Theodorsen's theory provides a useful approximation to the unsteady wake beneath the hovering rotor. The geometry for Loewy's theory is illustrated by Fig. 7. In this theory the effect of the spiral returning wake beneath the rotor is taken into account approximately. The wakes, infinite in number, lie in planes parallel to the disc of the rotor, these wakes are associated with both, previous blades (for an N-bladed rotor) and previous revolutions. The non-dimensional wake spacing $\bar{h}_w = h_w/b$, is determined by the rate at which the plane vortex sheets (representing approximately helical vortex sheets of the rotor) are convected downwards. Using the mean induced velocity at the rotor disc for the convection velocity of the wake near the rotor disc, the non-dimensional wake spacing is given by $\bar{h}_w = (2\pi v_i/\Omega Nb) = 4\bar{\lambda}/\sigma$.

The airfoil dynamics, assumed by this theory are identical to the simple harmonic pitch and plunge motion postulated in Theodorsen's theroy (see Fig. 6). Loewy has shown that for this case the unsteady aerodynamic lift and moment can be written in a form identical to Theodorsen's theory, except that C(k) is replaced by a more complicated lift deficiency function given by $C'(k,m,\bar{h}_w)$ where m is the frequency ratio $m = \omega/\Omega$. Combination of this lift deficiency function with Greenberg's theory[51] yields an approximate modified theory which provides an indication of some unsteady aerodynamic effects in hover, for a blade undergoing coupled flap-lag-torsional dynamics.

Results illustrating the application of the various theories mentioned above to the coupled flap-lag-torsional aeroelastic stability of a hingeless rotor blade in hover have been presented in Refs. 51 and 58. Figure 8, taken from Ref. 58, shows the sensitivity of the aeroelastic stability boundaries in hover to changes in two dimensional unsteady aerodynamic models.

A hingeless rotor model is used with a coupled flap-lag-torsional analysis based upon two rotating uncoupled normal modes for each elastic degree of freedom respectively. The results for a blade with $C_{do} = 0.01$; $a = 2\pi$; $\sigma = 0.08$; $\gamma = 8.0$; $b/R = 0.0313$; $R_c = 1.0$ and an offset $(x_A/b) = 0.20$ are depicted in Fig. 8. Two separate branches are typical of such stability boundaries. The branches extending to the left of the vertical broken line on the plot (representing a matched stiffness configuration) are the flap-lag stability boundaries in hover[1,51]. A flap-lag boundary usually involves only coupling between the fundamental flap and lag frequencies of the blade. Three separate curves are shown. The full curve representing quasisteady aerodynamics with apparent mass terms neglected, the broken line corresponding to Theodorsen's theory, with modification[51], and the third curve corresponding to Loewy's theory. The effect of apparent mass terms on these branches is quite pronounced, the influence of unsteady aerodynamics and the wakes beneath the rotor is small, but still evident. The branches on the right hand side of the plot (to the right of the matched stiffness vertical line) are stability boundaries in which the torsional degree of freedom also participates, in addition to the flap and lag degrees of freedom. The upper boundary due to the presence of the large x_A offset. The two narrow fingerlike regions of instability occur only when using a Loewy type unsteady aerodynamics. These regions are not evident when using Theodorsen type aerodynamics with Greenberg's modification. Thus they are due to the incorporation of the effect of unsteady wakes beneath the rotor. In these fingerlike regions, second flap and second lag modes couple with the torsional degree of freedom to produce the

unstable regions. Another interesting feature apparent from Fig. 8 is that the use of quasisteady aerodynamics with apparent mass effects neglected produces a stability boundary which tends to be conservative for this particular configuration. Other results, not presented here, indicate that for collective pitch angles in excess of 10°, the unsteady aerodynamic effects approach a quasisteady limit.

Furthermore, it should be noted that Loewy's theory has been extended to include compressibility effects by Jones and Rao[59] and Hammond and Pierce[60]. Additional material on this subject can be found in Ref. 61. Results illustrating the effects of compressibility on coupled flap-lag-torsional aeroelastic stability boundaries in hover are also available[51,58].

Another simple and convenient representation of rotor unsteady aerodynamics useful in aeroelastic analyses can be obtained by using a perturbation inflow model for rotor unsteady aerodynamics which is frequently denoted by the term dynamic inflow[4,62]. In this theory the inflow is written as a combination of steady inflow and a perturbation

$$\lambda(r,\psi) = \bar{\lambda} + \delta\lambda \tag{7}$$

and

$$\delta\lambda = \lambda_o + \lambda_c r\cos\psi + \lambda_s r\sin\psi \tag{8}$$

where λ_o, λ_c, λ_s are components of the dynamic inflow perturbation which are assumed to vary linearly over the disc.

Using a differential form of induced velocity solution of vortex or momentum theory the dynamic inflow components can be related to net unsteady aerodynamic forces and moments on the rotor, specifically the thrust C_T, the pitching moment C_{MY} and the rolling moment C_{MX}. The theory of dynamic inflow requires differential equations (or equations of motion), for λ_o, λ_s and λ_c because these quantities, which are coupled with the unsteady aerodynamic hub reactions, assume the role of additional degrees of freedom. These equations are usually written in the form[62]

$$[m]\begin{Bmatrix}\dot{\lambda}_o\\ \dot{\lambda}_s\\ \dot{\lambda}_c\end{Bmatrix} + [L]^{-1}\begin{Bmatrix}\lambda_o\\ \lambda_s\\ \lambda_c\end{Bmatrix} = \begin{Bmatrix}C_T\\ -C_{MX}\\ -C_{MY}\end{Bmatrix} \tag{9}$$

for simple momentum theory [m] and [L] are diagonal, for other theories they can be fully populated. The elements of these matrices have been also determined by using experimental measurements combined with system identification theory[63,64].

It is important to note that this model is based on the assumption that dynamic inflow is related to the aerodynamic loads in a linear, first order fashion. It has the capability of introducing into the aerodynamic loads a time delay, a low frequency approximation to lift deficiency and apparent mass effects. When dynamic inflow is coupled to the equations of blade dynamics it introduces an approximation to unsteady aerodynamic effects avoiding the complexity of more elaborate unsteady aerodynamic models, such as unsteady airfoil theory.

2.4.2 Forward Flight

Forward flight introduces some additional, substantial, difficulties in the aerodynamic modeling process. Figure 9 illustrates, in a simplified manner, the sources of these additional effects. Two important ingredients are the reversed flow region on the retreating blade and the dynamic stall which normally occurs in the vicinity of the reversed flow region. Additional important unsteady aerodynamic effects are due to unsteady transonic loads acting at the tip of the advancing blade. Obviously the precise formulation of the unsteady aerodynamic loading environment in forward flight is less developed than its counterpart for hover.

The aerodynamic modeling proglem, in absence of stall effects is considered first.

The simplest approach for this case is to use a quasisteady version of Theodorsen's or Greenberg's strip theories, with appropriate inclusion of forward flight effects in the velocity components at the deformed blade cross section, and incorporation of reversed flow effects[29,30]. A more accurate representation of the aerodynamic loads can be developed by combining two dimensional unsteady airfoil theory, with additional corrections for compressibility and lifting line effects (Ref. 4, pp. 526-535) which was used by Johnson[22,23].

Recognizing that a corresponding extension of Loewy's theory to forward flight is not available an alternative approach is to introduce an approximation to unsteady aerodynamic effects by using a version of the dynamic inflow model, discussed previosuly, with appropriate modifications for forward flight. For the forward flight case the elements of the [m] and $[L]^{-1}$ matrices can be determined empirically from tests[65] or they can be evaluated by analytical considerations[66] based on unsteady actuator disc theory[67].

Another severe aerodynamic loading condition imposed on rotary-wing aircraft is due to transonic phenomena associated with the flow field around the advancing side of the rotor disc. The transonic effects on helicopter rotor blades have been reviewed in a recent paper by Huber and Mikulla[68]. Transonic tip effects can cause tracking difficulties and subharmonic oscillations at high speeds[69]. One of the most comprehensive studies of the flow over a helicopter blade tip in the unsteady transonic regime was done by Carradona and Philippe[70] who have employed both experimental and computational techniques. The computations were based upon a two-dimensional transonic small disturbance equation. It is remarkable that the agreement between computation and experiment was good, since one would have expected three dimensional effects to be important at the blade tip. The results also indicated that unsteadiness is an important part of the problem. It was also noted[70] that the computations indicated great sensitivity to angle of attack variations. Since blade dynamics and flexibility can be represented as variations in effective angle of attack sensed by the moving cross section, it appears essential to couple blade dynamics to such unsteady aerodynamic flow calculations. Since the calculations done in Ref. 70 were for a nonlifting rotor it is worthwhile noting that steady transonic calculations on a lifting rotor have been also reported recently[71].

Aerodynamic modeling in presence of stall is considered next. Dynamic stall is a strong nonlinear unsteady aerodynamic effect which plays a major role in aeroelastic stability and response calculations. This topic is also reviewed in detail in Ch. 16 of Ref. 4. Dynamic stall is associated with the retreating blade and borders on the reversed flow region, as shown in Figure 9,

a more accurate description of the angle of attack distributions on a high speed rotor are shown in Fig. 4 of Ref. 61. Under these conditions the angle of attack of the blade section is periodically very large when the blade is on the retreating side. An indication of the severe aerodynamic loading conditions in such regions are evident from Fig. 10, taken from a recent paper by Gangwani[72]. Under normal flight conditions the torsional response of the blade is relatively low, however at the flight envelope boundary, where dynamic stall effects are pronounced, large transient torsional excursions may be excited accompanied by low negative damping in pitch. This source generates excessive control system and blade vibratory loads which impose speed and load limitations on the rotor system as a whole. It can also cause stall-flutter. Due to the importance of the dynamic stall phenomenon it has been the subject of a vast number of studies which have resulted in a relatively good physical understanding of this complex, unsteady aerodynamic effect. The work of McCroskey and his associates[73-75] has led to a good physical understanding of this phenomenon using experimental and analytical techniques. A recent study my Mehta[76] is an impressive illustration of additional understanding of dynamic stall which can be gained by judicious use of computational fluid mechanics. The complexity of such models however preclude their incorporation in conventional rotary wing aeroelastic analyses. Therefore numerous semiempirical models have been developed which are aimed at including this effect in aeroelastic stability and response calculations[4]. The purpose of this section is to review three such recent methods which seem to have considerable potential for application to rotary-wing aeroelasticity[72,77-79].

The principal features of dynamic stall of an oscillating airfoil are flow separation, formation of a leading edge vortex (or vortices) and passage of the vortex (or vortices) over the airfoil surface. The secondary features such as strength or vortex (or vortices), location, instant of formation and the number of vortices depend upon the airfoil geometry, frequency of oscillation, amplitude of oscillation and Reynolds number. These principal and secondary features together determine the aerodynamic characteristics of the oscillating airfoil[76].

The vortex formation and passage model commonly used in dynamic stall analyses is schematically illustrated in Fig. 11. When the airfoil experiences an unsteady increase in angle of attack beyond the static stall angle, a vortex starts to grow near the leading edge region. As the angle continues to increase, the vortex detaches from the leading edge and is convected downstream near the surface. These events are shown schematically in Fig. 11, taken from Ref. 72. The suction associated with the vortex normally causes an initial increase in lift. The magnitude of the increase depends on the strength of the vortex and its distance from the surface. The streamwise movement of the vortex depends on the airfoil shape and the rate of pitch. The relative distance between the vortex and the airfoil depends on the dynamics of the airfoil. That is, it depends on the pitch rate, the instantaneous effective angle of attack, etc. As the vortex leaves the trailing edge, a peak negative pitching moment is obtained. The airfoil then remains stalled until the angle of attack drops sufficiently so that reattachment of the flow can occur.

The various methods for incorporating dynamic stall in rotary wing aeroelastic calculations, to be described below, are based on the preceding physical model. These methods have a number of common features:

(a) A common goal, which is the incorporation of section unsteady aerodynamic effects into a theoretical analyses of rotordynamics. Since such analysis are usually performed in a stepwise manner in the time domain they utilize a time domain representation of the section unsteady aerodynamics.

(b) All models are empirical, i.e. various parameters in the model are determined by fitting the theory to experimental data obtained from oscillating airfoil tests.

(c) The details of the methods are rarely presented in a complete manner, which frequently causes difficulties to a potential user who is interested in implementing the methods in an aeroelastic calculation.

A brief description of the main features of these dynamic stall models is provided below:

Beddoes Model[77] is the most convenient to use. It is computationally efficient and does not require excessive amount of computer time. Continuity is maintained in the timewise variation of the attached and separated flow regions. Totally arbitrary forcing function may be handled in a stepwise manner. Phasing and magnitude of high pitching moment and normal force coefficients on the airfoil, resulting from separated flow can be reproduced. However, it does not seem to have any provision for generating unsteady drag data. It is based on experimentally derived static airfoil characteristics.

The model and the subsequent analysis consist of two distinct flow regimes: the attached flow regime and the separated flow regime.

In the attached flow regime Wagner's indicial function[49], generalized for compressible flow, is used to generate the unsteady lift and moment. This approach leads itself conveniently to stepwise loading calculations in which the azimuth interval is the independent variable. For example the lift is generated by

$$C_L = C_{L\alpha}\Delta\alpha\Phi(s) = C_{L\alpha}\alpha_E(s) \tag{10}$$

$$\Phi(s) = 1 - A_1 e^{-b_1 s} - A_2 e^{-b_2 s} \tag{11}$$

where $\Phi(s)$ is the Wagner function and $s = 2tU/c$ is a nondimensional time variable. It should be noted that Wagner's function represents a typical fixed wing type of wake. This function is evaluated in a stepwise manner in the time domain.

In the separated flow region, a physical model based on the observation of a large amount of experimental data is assumed. The static lift (C_N) is idealized in a segmented manner. The static moment (C_M) is also idealized in a segmented manner using the movement of the center of pressure. Finite time delays, based on observation of experimental data are introduced to simulate onset of pitching moment and lift divergence. A progressive, linear, movement of the center of pressure to its fully separated value is assumed. An exponential decay of lift at stall is also assumed. Finally reattachment of flow at moderate angles of attack is introduced.

This model has proven itself quite capable of reproducing experimentally obtained C_N and C_M coefficients for a wide range of reduced frequencies k, Mach numbers, and various types of airfoil motion such as pitch and plunge, as well as response to ramp type airfoil motions. Typical results, taken from Ref. 77 are shown in Fig. 12 which illustrates how the relation between pitching moment and lift divergence time-delays influence the damping and maximum C_M. Considering each cycle shown in the figure, the mean angle of attack α_{MEAN} increases progressively. The first ($\alpha_{MEAN} = 4.8°$) shows only very

limited separation which, however, is sufficient to introduce a small loop of negative damping. The second cycle shows earlier C_M divergence which increases the loop negative damping reducing the overall value to close to zero. Further increase of mean angle introduces an extra loop of positive damping, this is due to the center of pressure having reached the fully separated value before the end of the cycle. Maximum pitching moment is now a function of C_{LMAX} which occurs earlier in the cycle and thus offsets the effect of increasing mean angle.

Figure 13, also taken from Ref. 77, shows how increasing frequency can allow more of the cycle to be completed before the onset of separation effects. In this particular case, it has the effect of initially driving the damping to more negative values and then subsequently in the direction of positive damping. The maximum values of pitching moment still occurs at the point of lift divergence which, at higher frequencies, is delayed to lower angles in the return part of the cycle. Thus maximum C_M is no longer a function of the maximum lift. These data seem to indicate a delay in reattachment at high frequency.

These results also indicate that agreement between test results and the semiempirical model are not uniformly good. This gives credibility to the assertion[76] that these simplified methods are inferior to the results which can be obtained by computational fluid mechanics.

Gangwani's Model[72] has certain similarities to Beddoes model particularly in its treatment of the attached flow region. This model also generates the unsteady aerodynamic forces in the time domain, utilizing three parameters: (1) the instantaneous angle of attach $\alpha(t)$, (2) the nondimensional pitch rate $A = c\dot{\alpha}/2U$ and (3) a parameter $\alpha_W = \alpha(s) - \alpha_E(s)$, which accounts for the time effects in change of α based on Wagner's function corrected for compressibility.

The treatment of the attached flow regime in this model is very similar to Beddoes[77].

The treatment of the separated flow regime is substantially different from Beddoes model, although some similarities exist. The key ingredients in the model are the prediction of the onset of dynamic stall and center of pressure movement due to vortex motion. The angle α_E at the onset of stall is determined from an approximate linearized relation which depends on a constant which can be determined from test data. The instant when the vortex, detached from the leading edge, leaves the trailing edge is also determined from an empirical relation somewhat similar to Beddoes model. Reattachment is assumed to occur at the angle of static stall. The unsteady lift, pitching moment and drag coefficients denoted respectively by C_{LU}, C_{MU} and C_{DU} are expressed in analytical form which depends on over twenty undetermined coefficients. Subsequently these undetermined coefficients are calculated by least squares curve fitting of these coefficients with experimental data obtained from oscillating airfoil tests. Since numerous techniques for least squares curve fitting exist[80] the accuracy of the method depends, to some extent, on the particular least square technique employed. The important effect of sweep is incorporated in Gangwani's model.

Comparison of synthesized loop data, obtained from this model, with test data indicate good overall agreement. The comparison of synthesized C_L(or C_N) loop with test data is illustrated in Fig. 14 taken from Gangwani's paper[72]. The differences between the test data and the synthesized data are small and comparable to test data accuracy. The comparison of synthesized C_M loops with test data is shown in Fig. 15. Again the correlation between theory and test is good. The maximum negative C_M value, which is important for blade response calculations, is always predicted accurately for all the stalled loops. One apparent slight difficulty is the prediction of the instant when reattachment occurs. The synthesized moments loops presented in Fig. 15 are based on the assumption that reattachment occurs when α approaches the static stall angle. Replacement of this assumption by a better criterion for reattachment could lead to further improvement in the correlation between this theory and test data.

It is also interesting to note that while the theoretical model presented by Gangwani contains the appropriate expressions for the unsteady drag coefficient C_{DU}, no results for this quantity are presented in this paper. It is well known that the lead-lag degree of freedom is important in rotary-wing aeroelasticity, therefore it would have been very interesting if synthesized loop data for C_{DU} would have also been presented.

Dat, Tran and Petot's Model[78,79] is also based on the time domain representation of the airfoil section operating before, during and in the post stall regime while it performs essentially arbitrary motions.

This model also distinguishes between the attached and stalled flow regimes. The method utilizes basic properties of differential equations to simulate time history, or hysteresis, of flow; by taking advantage of the properties of real and complex poles to simulate time delays.

The method is based on a number of assumptions. It is assumed that large amplitude motions occur at low frequencies, while small amplitude motions occur only at high frequencies. It is also assumed that the difference between unsteady aerodynamic forces and the static ones are of relatively small quantities. Static forces are obtained from static tests. The model seems to represent a version of the unsteady aerodynamic forces linearized about a set of static nonlinear forces. This model also contains a number of undetermined coefficients which are subsequently identified by using least squares system identification methods. In this identification process only high frequency, low amplitude oscillations are used for identification purposes. Measurements conducted with airfoils with large amplitude oscillations are not used for identification purposes, but serve to check the validty of the model after identification. The results, presented in Refs. 78 and 79, for synthesized loop data for the normal force coefficient C_N and the moment coefficient C_M, indicate reasonable agreement with test data. The agreement between theory and test appears to be somewhat better than in Figs. 12 and 13, but not as good as the agreement evident in Figs. 14 and 15.

When comparing these dynamic stall models, it is evident that all three models use a very similar approach in dealing with the attached flow regime, however they differ in the treatment of the separated flow regime. The second[72] and third[78,79] model, described above, represent essentially improvements upon Beddoes model. The improvements are accomplished by refining

the model in the separated flow regime. Both methods accomplish this improvement by introducing parameters into the model which are subsequently identified, using least squares system identification, by fitting the model to experimental data obtained on oscillating airfoil tests. Beddoes model relies more heavily on static airfoil characteristics and does not utilize system identification techniques.

The effect of incorporating such dynamic stall models in aeroelastic response calculations will be discussed in a latter portion of this paper.

Finally it should be noted that dynamic airfoil tests which are used to compare with synthesized loop data are normally generated for pitch and plunge type motions. Since the lag degree of freedom has proven itself to be important in aeroelastic stability analyses[1], the effect of inplane motion and consequent variation in the relative freestream velocity could have an influence on airfoil dynamic stall characteristics[81].

2.5 Ordering Schemes

As indicated in Section 2.2 an important ingredient in modeling rotary-wing aeroelastic problems is the incorporation of geometrical nonlinearities due to the assumption of small strains and moderate deflections. When these geometrical nonlinearities are incorporated in the inertia (Section 2.3) and aerodynamic (Section 2.4) operators associated with the rotary-wing aeroelastic problem they give rise to numerous higher order nonlinear terms. Ordering schemes provide an effective mechanism for neglecting higher order nonlinear terms in a consistent manner and enable one to achieve substantial reduction in the algebraic size of the final dynamic equations of equilibrium. Therefore ordering schemes have been used in a majority of recent studies in which geometrically nonlinear blade models were considered[1,24,29,30,42,82,83,85-88].

Ordering schemes are based on assigning orders of magnitude to the various physical parameters, governing the aeroelastic problem, in terms of the elastic blade slopes which are assumed to be moderate, i.e. blade slopes are assumed to be of order ε, with $0.10 < \varepsilon < 0.20$. The higher order nonlinear terms in the resulting equations of dynamic equilibrium are neglected by assuming

$$O(1) + O(\varepsilon^2) \cong O(1) \tag{12}$$

Consider as an example the treatment of the coupled flap-lag-torsional dynamics of an isolated blade in forward flight[29]. For this case the ordering scheme would be based on the order of magnitude assignments given below.

$$w_{,x} = v_{,x} = \phi = O(\varepsilon)$$

$$\frac{e_1}{R} = \frac{b}{R} = \beta_p = \bar{\lambda} = \lambda_{1s} = \lambda_{1c} = \frac{w}{R} = \frac{v}{R} = O(\varepsilon)$$

$$\theta = \theta_{1c} = \theta_{1s} = O(\varepsilon^{1/2})$$

$$u = x_I/R = x_A/R = O(\varepsilon^2) \; ; \; C_{do}/a = O(\varepsilon^{3/2})$$

$$x/\ell = \frac{\partial}{\partial x} = \frac{\partial}{\partial \psi} = \mu = O(1)$$

Application of such an ordering scheme leads to the neglect of numerous higher order terms. Furthermore the method is equally useful in presence of dynamic stall effects. Finally it should be noted that such a scheme is based on common sense and experience with practical blade configurations, thus it should be applied with a certain degree of flexibility.

2.6 Equations of Dynamic Equilibrium

Combination of the structural, inertia and aerodynamic operators described above, together with an appropriate representation of viscous or structural damping effects[1,29] yields the dynamic equations of equilibrium, after applying the ordering scheme. The equilibrium equations are, usually, nonlinear partial differential equations, depending on both space and time variables. In the case of forward flight the equations have periodic coefficients in the azimuth (time) variable. A representative example of the complexity of such equations for the coupled flap-lag-torsional dynamics of a hingeless blade in forward flight is presented in Ref. 29.

3. Solution of Rotary-Wing Aeroelastic Problems for the Isolated Blade Case

3.1 Spatial Discretization

The first step in the solution of rotary-wing aeroelastic stability or response problems is elimination of the spatial dependence of the problem using a suitable discretization method. Application of such discretization methods to the nonlinear partial differential equations of dynamic equilibrium will yield a set of coupled nonlinear ordinary differential equations.

3.1.1 Spatial Discretization Based on Global Modes

A conventional method for discretizing rotary-wing aeroelastic equations, which has been frequently used in the past, consisted of applying the well known Rayleigh-Ritz method or extended Galerkin method[1,24,25,34] based upon the free vibration modes of a rotating blade. Due to the fact that the partial differential equations are nonlinear the extended Galerkin method is somewhat more convenient to use. For the case of hover both coupled[24] and uncoupled modes[1,58,83] have been used. Uncoupled modes are those obtained by solving the free vibration problem of a rotating beam separately in the flap, lag and torsional degrees of freedom respectively. Coupled modes are those obtained from solving the coupled flap-lag-torsional free vibration problem of a rotating beam[24]. There is a slight, but not substantial advantage, in using coupled modes, since slightly better convergence of the results is obtained. However for analyses intended for both hover and forward flight coupled modes are both inconvenient and inaccurate, because the time varying cyclic pitch introduces periodic coefficients into the free vibration problem by virtue of the elastic coupling or structural coupling terms[1,24]. Therefore for forward flight problems the use of uncoupled modes[25] is more convenient. This problem is also illustrated by a recent paper by Hansford[84], where special approximations had to be introduced to define coupled modes about an average pitch angle.

Both the Galerkin or the Rayleigh-Ritz method imply a modal expansion for the flap-lag and torsional degrees of freedom given by

$$w = \sum_{i=1}^{n_F} \ell g_i(\psi)\ \eta_i(\bar{x}_o)$$

$$v = -\sum_{j=1}^{n_L} \ell h_j(\psi)\ \gamma_j(\bar{x}_o)$$

$$\phi = \sum_{k=1}^{n_T} f_k(\psi)\ \phi_k(\bar{x}_o) \qquad (13)$$

Implementation of both methods leads to cumbersome algebraic manipulations, which have to be carried out manually or by alternative means such as algebraic manipulative systems. In some cases the amount of algebraic manipulations associated with such global methods is so excessive that it prohibits treatment of complicated blade configurations in a realistic manner.

Substitution of Eqs. (13) into the dynamic equations of equilibrium requires evaluations of numerous integrals. These are usually evaluated using Gaussian quadrature.

3.1.2 Spatial Discretization Based on Finite Element Methods

An alternative discretization method is based upon the finite element approach, which enables one to discretize the partial differential equations of motion directly. Consequently, a significant reduction in the algebraic manipulative labor required for the solution of the problem is accomplished. Furthermore the finite element method is ideally suited for modeling the complicated and redundant structural system encountered in a bearingless rotor, and can be applied with relative ease to both aeroelastic stability and response calculations. For rotary-wing aeroelastic problems two approaches have been used: (1) a weighted residual Galerkin type finite element method[85,86] and (2) a conventional local Rayleigh-Ritz finite element method[87]. The first method appears to be slightly more convenient for the aeroelastic stability or response problems in forward flight.

The geometry illustrating the application of a Galerkin type finite element method for the coupled flap-lag aeroelastic problem in hover and forward flight[85,86,88] is shown in Fig. 16. The complete coupled flap-lag-torsional problem in forward flight is also formulated in Ref. 88. The method is based on the partial differential equations of equilibrium, which are discretized directly, using a local weighted residual Galerkin method. As shown in Fig. 16, each element has four nodal degrees of freedom, representing flap and lag displacements and slopes respectively. The bending degrees of freedom are discretized using a conventional, beam type bending element, based on Hermite polynomials, i.e. cubic interpolation for bending. It is important to recognize that when modeling coupled bending torsion problems, quadratic interpolation for the torsional degree of freedom is required for consistency with this bending representation. Thus the torsional element would contribute an additional nodal degree of freedom to the element shown in Fig. 16, together with an additional internal node[86,88]. The element matrices obtained in this procedure are dependent on the nonlinear equilibrium

position, which also implies that in forward flight these element matrices are time dependent. The element matrices are assembled using a conventional direct stiffness method. After assembly, a normal mode transformation is used to reduce the number of nodal degrees of freedom. This approach leads to substantial savings in computer time. Numerous results illustrating the convergence properties of the method as well as blade behavior in hover and forward flight were presented[85,86,88]. The experience gained in these studies indicates conclusively that the Galerkin type finite element method is a practical tool for solving rotary-wing aeroelastic stability and response problems.

A local Rayleigh-Ritz type finite element method has been recently used by Sivaneri and Chopra[87] to study the coupled flap-lag-torsional aeroelastic stability problem in hover. The finite element formulation is based upon the principle of virtual work. While the bending representation is identical to Refs. 85, 86 and 88, the torsional representation is based on linear interpolation. This choice of interpolation orders is not consistent. Because cubic interpolation in bending allows for a quadratic variation of the integrand of the strain energy integral for bending, while linear interpolation in torsion gives rise to a constant integrand for the torsional strain energy. As a consequence the conclusions obtained in this study regarding the number of elements needed for convergence are somewhat inaccurate.

It is also worthwhile mentioning that finite element analyses have also been frequently used to solve the free vibration problem of rotating beams, a recent paper by Hodges and Rutkowski contains a relatively complete survey of this more restricted topic[89].

3.1.3 Spatial Discretization Based on Integrating Matrix Method

Another method for accomplishing spatial discretization is the integrating matrix method. This method has been used successfully for rotating blade vibration problems in both linear[90,91] and nonlinear formulations[92]. White[93] has also used the integrating matrix method for the coupled flap-pitch flutter analysis of a rotor blade in hover.

The integrating matrix method (IMM) is based on direct numerical integration. The integrating matrix may be viewed as a matrix operator which by premultiplying a vector, containing as elements the values of a function at discrete stations along the blade, transforms it into another vector having the integrals of the function (from one end of the blade to each station) as elements. To account for the boundary condition, a constant vector has to be added. In order to apply the IMM to the solution of a differential equation, it is necessary to write the differential equation or an integrated form of it, at a number of stations along the blade.

Derivation of the integrating matrix is based on piecewise polynomial interpolation. If, for convenience, equally spaced collocation points are chosen, Newton's forward-difference interpolation formula can be used to express the polynomial coefficients in terms of the function values at the appropriate collocation points. Integration of the polynomial expressions yields the elements of the integrating matrix.

The IMM always leads to nonsymmetric system matrices, even when considering a self-adjoint problem. Furthermore, the matrices are not banded. The eigenvectors (for free vibration problems) are not orthogonal with respect to the system matrices. Furthermore, the IMM does not yield upper bound solutions. Finally, for free vibration problems, the dynamic matrix is degenerate, leading to zero eigenvalues which correspond to infinite frequencies. Consequently finite element methods are superior to IMM methods as a discretization tool for rotary-wing aeroelastic problems.

3.2 Solution of the Blade Dynamics Problem in the Time Domain

3.2.1 General

The discretization process, described in the previous section, reduces the nonlinear, coupled, partial differential equations to nonlinear ordinary differential form. For the general case of forward flight, these coupled ordinary differential equations also have periodic coefficients. The mathematical structure of these general equations can be presented in the following symbolic form

$$[M]\{\ddot{X}\} + [C(\psi)]\{\dot{X}\} + [K(\psi)]\{X\} = \{F_{NL}(\psi, \underset{\sim}{X}, \dot{\underset{\sim}{X}})\} \tag{14}$$

where it is understood that the matrices [M] and [C(ψ)] contain both aerodynamic and inertial contributions, while the matrix [K(ψ)] contains aerodynamic, inertia as well as structural contributions. In this, general, formulation all nonlinear effects and the excitation are combined in a general vector $\{F_{NL}(\psi, \underset{\sim}{X}, \dot{\underset{\sim}{X}})$. When dynamic inflow is considered, Eqs. (9) have to be appended to Eqs. (14) and solved jointly[62]. In discussing methods for solution of Eqs. (14) it is convenient to consider two separate flight regimes, namely: (1) hover and (2) forward flight.

3.2.2 Hover

For the isolated blade case, in absence of dynamic inflow effects, the problem reduces to a nonlinear system, with constant coefficients represented by

$$[M]\{\ddot{X}\} + [C]\{\dot{X}\} + [K]\{X\} = \{F_{NL}(\underset{\sim}{X}, \dot{\underset{\sim}{X}})\} \tag{15}$$

In this case aeroelastic stability is usually the more important problem. Assuming quasisteady aerodynamics and no stall effects, and linearizing these equations about a nonlinear equilibrium position, gives a good approximation to the aeroelastic stability boundaries[1,24,83,85-88].

Using perturbation equations about the equilibrium state

$$\{X(\psi)\} = \{X_o\} + \{\Delta X(\psi)\} \tag{16}$$

and neglecting terms which are nonlinear in terms of the perturbation quantities, i.e., $\Delta X_i(\psi)\Delta X_j(\psi)$, yields two separate equations

$$[S]\{X_o\} = \{L_S\} + \{F_{SN}(\underset{\sim}{X}_o)\} \tag{17}$$

$$[M]\{\Delta\ddot{X}(\psi)\} + [C(\underset{\sim}{X}_o)]\{\Delta\dot{X}(\psi)\} + [K(\underset{\sim}{X}_o)]\{\Delta X(\psi)\} = \{0\} \quad (18)$$

Equation (17) is a system of nonlinear algebraic equation which yields the static equilibrium position. These equations are usually solved by Newton-Raphson iteration[1,24,83,85,88] although other methods, such as shooting methods have also been used[94].

Equation (18) is linear in the perturbation quantities, however its coefficients depend on the static equilibrium position obtained from Eq. (17). It is convenient to rewrite Eq. (18) in first order state variable form[1,24,83-88] where

$$\{y(\psi)\} = \begin{Bmatrix} \Delta\dot{\underset{\sim}{X}}(\psi) \\ \Delta\underset{\sim}{X}(\psi) \end{Bmatrix} \quad (19)$$

which reduces Eq. (18) to the standard eigenvalue problem

$$[A]\{Y\} = \lambda\{y\} \quad (20)$$

The real part of the eigenvalues λ_i determine the aeroelastic stability boundaries of the blade.

For the sake of completeness a number of other situations which can occur in hover and do not follow exactly the preceding treatment are also mentioned. When unsteady aerodynamics of a rotary-wing type, such as Loewy's are used, Eq. (17) still applies, however the perturbation equations have to be solved in an iterative modification of a conventional V-g method[51]. When static stall effects are present, an approximation based on perturbation equations about an appropriate equilibrium position, generated stability boundaries, which predicted the stall-induced flap-lag instability quite well[47].

3.2.3 Forward Flight

The aeroelastic stability or response problem is based upon Eqs. (14). When dynamic stall effects are neglected, reliable solutions for stability or response can be obtained by linearizing the nonlinear equations of motion about an appropriate equilibrium position[25]. In forward flight the appropriate equilibrium position is a time dependent periodic solution. Calculation of the time dependent periodic equilibrium position, representing the response solution of the blade is inherently coupled with the trim state of the complete helicopter in forward flight. The degree of sophistication with which this coupling is accomplished can affect the accuracy of the aeroelastic analysis[25,95].

In practice two trim calculations are required[25,95], as illustrated schematically in Fig. 17: (1) Propulsive Trim, which simulates actual forward flight conditions. The weight coefficient C_W (approximately equal to the thrust coefficient) is specified, and horizontal and vertical force equilibrium is maintained. Zero pitching and rolling moments are enforced; (2) Moment or Wind Tunnel Trim, simulates conditions under which a rotor would be tested in a wind tunnel. Horizontal and vertical force equilibrium is not enforced because the helicopter is mounted on a supporting structure. Therefore, only the requirement of zero moments on the rotor is imposed.

Two methods for generating solutions to Eqs. (14) are available. The first approach is based on the direct treatment of the blade equations, in the rotating system, and uses the theory of differential equations with periodic coefficients. The second approach introduces a coordinate transformation from the rotating blade fixed coordinate system to a hub fixed, nonrotating, coordinate system. Both approaches are described below.

The direct approach to solution of Eqs. (14) is facilitated by rewriting them in first order state variable form. When using this representation, Eqs. (14) can be rewritten as[25]

$$\{\dot{q}(\psi)\} = \{Z(\psi)\} + [L(\psi)]\{q(\psi)\} + \{N(\underset{\sim}{q},\psi)\} = \{F_{NL}(\psi,\underset{\sim}{q},\dot{\underset{\sim}{q}})\} \tag{21}$$

where it is understood that the system is periodic with a common period of 2π, i.e.

$$\{Z(\psi)\} = \{Z(\psi+2\pi)\}$$

$$[L(\psi)] = [L(\psi+2\pi)] \tag{22}$$

and

$$\{q(\psi)\} = \begin{Bmatrix} \dot{X}(\psi) \\ \\ \underset{\sim}{X}(\psi) \end{Bmatrix} \tag{23}$$

It is important to note that in all rotary-wing aeroelastic problems, in presence of forward flight, the response and stability problems are coupled. Therefore solutions have to be obtained in two stages[25]: first the nonlinear time dependent equilibrium position of the blade is obtained, and next the equations are linearized about the time dependent equilibrium state by writing perturbation equations about the nonlinear equilibrium position. This second stage, yields a set of linearized perturbation equations with periodic coefficients from which blade stability is obtained using Floquet theory.

In this approach the linear portion of Eq. (21) is considered first

$$\{\dot{q}_L(\psi)\} = \{Z(\psi)\} + [L(\psi)]\{q_L(\psi)\} \tag{24}$$

together with the associated homogeneous equation

$$\{\dot{q}_H(\psi)\} = [L(\psi)]\{q_H(\psi)\} \tag{25}$$

For a stable homogeneous system, Eq. (24), has only one periodic solution given by

$$\{q_L(\psi)\} = [\Phi(\psi)]\Big\langle \int_o^{\psi} [\Phi(s)]^{-1}\{Z(s)\}ds + \left([I] - [\Phi(2\pi)]^{-1}\,[\Phi(2\pi)] \int_o^{2\pi} [\Phi(s)]^{-1}\{Z(s)\}ds\right) \Big\rangle \tag{26}$$

A general solution of any inhomogeneous system, like Eq. (24), whether periodic or not is given by

$$\{q_L(\psi)\} = [\Phi(\psi)]<\int_o^{\psi} [\Phi(s)]^{-1}\{Z(s)\}ds + \{q(0)\} > \qquad (27)$$

where the underlined term in Eq. (26) simply represents the initial condition $\{q(0)\}$ in Eq. (27) which gives a periodic response. Thus the periodic steady-state solution can be obtained by numerically integrating the linear system, Eq. (24), with this initial condition[25,96]. Normally, excellent converged solutions are obtained within two or three rotor revolutions, using a fourth order Runge-Kutta method with Gill coefficients. Reference 97 contains a slightly different formulation for obtaining the steady-state response of a linear periodic system.

Solution of the complete nonlinear system, Eq. (21), is based on quasilinearization[25]. Doing a first order Taylor series expansion of Eq. (21) about the k^{th} iterate yields

$$\{\dot{q}\}^{k+1} = \{F_{NL}\}^k + \left[\frac{\partial \underset{\sim}{F}_{NL}}{\partial \underset{\sim}{q}}\right]^k (\{q\}^{k+1} - \{q\}^k) +$$

$$+ \left[\frac{\partial \underset{\sim}{F}_{NL}}{\partial \underset{\sim}{q}}\right]^k (\{\dot{q}\}^{k+1} - \{\dot{q}\}^k)$$

which can be also written as

$$\{\dot{q}\}^{k+1} = [A(\psi)]^k \{q\}^k + \{f\}^k \qquad (28)$$

Thus, Eq. (28) represents a sequence of linear response iterates in a quasilinarization sequence. The iteration is terminated when

$$|\{q\}^{k+1} - \{q^{(k)}\}| < \varepsilon_{QL} \qquad (29)$$

This converged solution represents the nonlinear periodic equilibrium position about which the equations are linearized.

Once the time dependent equilibrium position has been established, the system represented by Eq. (21) is perturbed about this equilibrium position

$$\{q(\psi)\} = \{\bar{q}(\psi)\} + \{\Delta q(\psi)\} \qquad (30)$$

where squares of perturbation quantities are neglected and the stability of the linearized system is determined from Floquet theory by evaluation of the characteristic exponents[4,95]

$$\lambda_k = \zeta_k + i\omega_k \tag{31}$$

The linearized system is stable when $\zeta_k < 0$.

In this context it should be also mentioned that a key ingredient in dealing with period systems is the efficient numerical computation of transition matrices which has been treated in Ref. 98. Another recent study has compared a variety of methods for computing transition matrices for rotorcraft[99]. This study was based on comparing a number of available canned routines, which is not a reliable basis for comparison studies[98], thus the results obtained were somewhat inconclusive.

As indicated the nonlinear time dependent equilibrium position is intimately coupled with the global equilibrium or trim condition of the complete helicopter. Thus an aeroelastic stability or response calculation might also require an iterative application of trim conditions. Such an approach was considered in Ref. 88, and found to be computationally very expensive. Finally, it should be noted that the method of analysis described in this section proved itself to be compatible with a finite element blade representation for forward flight aeroelastic stability and response calculations[86,88].

A second approach to the solution of Eqs. (14) is based upon the introduction of a Fourier type coordinate transformation which transforms the variables $\{X\}$ from the rotating, blade fixed reference frame, to a nonrotating hub fixed reference frame. Following Hohenemser[100] these coordinates are frequently used in rotordynamics[4,45,46,62,101,102,103]. Use of such a coordinate transformation implies that the blade degrees of freedom, in the blade fixed coordinate system, are replaced by a set of nonrotating coordinates fixed in the hub, which describe the motions of the hub plane, and its deformation in a hub fixed system. In a symbolic form the multiblade coordinate transformation can be written as

$$\{X\} = [B(\psi)]\{Y\} \tag{32}$$

where $\{X\}$ are the original coordinates in Eq. (14) and $\{Y\}$ are the multiblade coordinates[62,101]. The multiblade transformation is somewhat difficult to use when the equations contain numerous geometrical nonlinear terms, such as the coupled flap-lag-torsion equations in forward flight[29] and even for the coupled flap-lag case the algebraic effort can be substantial[101]. However, when applicable the multiblade coordinates have some convenient features. For low advance ratios, $\mu < 0.25$, and rotors having three or more blades, use of a transformation such as Eq. (32) on Eqs. (14) enables one to neglect the periodic coefficients in the transformed equations. Thus the system becomes a constant coefficient system which can be easily treated by conventional methods. For higher advance ratios it is still possible to use multiblade coordinates, and treat the remaining periodic coefficients by averaging or harmonic balancing methods as pointed out in a recent review study by Dungundji and Wendell[104].

When dynamic inflow effects are incorporated into the treatment of forward flight problem, Eqs. (9) are appended to Eqs. (14) and solved jointly[62, 101].

Solution of the aeroelastic stability and response problem in presence of dynamic stall is somewhat more complicated. In this case, Eqs. (14) still represents the appropriate system of equations which are to be solved. However, the strong nonlinear aerodynamic effects introduced by dynamic stall might

preclude the use of quasilinearization technique such as described in the first part of this section. The conventional method used in this case is direct numerical integration, of Eqs. (14), in the time domain[72,77]. Two methods of numerical integration are available: (1) direct integration schemes which have been developed for structural dynamics response problems, when formulated in conventional second order form, i.e. Eqs. (14), such as the Houbolt, Wilson and Newmark methods[105] or (2) conventional direct numerical schemes such as Runge-Kutta or predictor corrector methods[106,107] which are intended to be used when the equations are written in first order form, i.e. Eqs. (21). Both methods have advantages and disadvantages. Furthermore, the appropriate step size has to be determined from numerical experimentation, since the equations are both nonlinear and have periodic coefficients.

Tran and Falchero[108] have used an alternative approach to direct numerical integration in a recent study which incorporated the dynamic stall model, discussed in Section 2.4.2, in a blade response calculation. The response of the blade was evaluated by using a matrix exponential approximation[101,110] to evaluate the transition matrix, during a small interval of the blade revolution.

3.3 Isolated Blade Stability and Response, Some Illustrative Results

The results presented are intended to complement the material provided in previous sections by serving as illustrative examples for the analytical techniques which have been discussed.

Consider first results in hover. Figure 18 shows typical results obtained for a coupled flap-lag model of a hingeless blade[85], with quasi-steady aerodynamics and uniform inflow in hover. The geometry for this finite element model was shown in Fig. 16. The analysis for this case follows the outline presented in Section 3.2.2. The blade is modeled using six elements and sensitivity of the results with respect to the number of modes used in the analysis is explored. Figure 18 also illustrates that for this case, there is practically no difference between the results based on using four or six beam type elements. The unstable parts of the stability boundary, where the real part of the eigenvalue is positive, are denoted by the letter U on the boundary. The number of modes, given next to each line, indicates the number of elastic modes used to represent each elastic degree of freedom. Thus two modes imply that two rotating uncoupled modes are used to represent the flap and lag degree of freedom respectively, (i.e. a total of four). These modes, generated from the finite element modes, are used to reduce the number of nodal degrees of freedom, in the finite element analysis of the aeroelastic problem[85]. The interesting results shown in this figure are the unstable regions associated with the second lag mode, which for intermediate values of the elastic coupling parameters $R_c = 0.60$, becomes unstable at lower values of the critical collective pitch angle θ_c than the first lag mode. For elastic coupling parameters $R_c = 0$, it is always the fundamental lag mode which yields the lowest stability boundary as shown in Fig. 18 and for $R_c = 1.0$, the flap-lag instability is virtually eliminated. These results, together with the stability results shown in Fig. 8 indicate, that for hingeless blade aeroelastic stability calculations at least two rotating elastic modes should be used to represent each elastic degree of freedom. For response and dynamic load calculations a somewhat larger number of modes would be required.

Results associated with forward flight are presented next. The first set of results, is representative of a coupled flap-lag-torsional stability analysis of a hingeless rotor blade in forward flight[25]. This analysis is

based on two elastic modes for each degree of freedom, i.e. flap, lag and torsion respectively, quasisteady aerodynamics and no stall effects. The analysis follows the outline presented in Section 3.2.3. Figures 19 through 22 illustrate the stability of a stiff-in-plane blade in forward flight. The parameter k on these plots represents the quasilinearization iteration index used in Eq. (28). The case K = 0 corresponds to a linear periodic response in which all nonlinear terms are neglected, the case k = 1 represents a linearized response, and k = 2 gives the first approximation of the fully nonlinear response. Since Figures 19 through 22 represent the real part of the characteristic exponent associated with a particular degree of freedom, plotted versus the advance ratio μ, they represent stability boundaries linearized about the corresponding equilibrium position.

Clearly, nonlinear terms have a marked effect on the blade stability. There is a strong degradation in stability with advance ratio for this case, Fig. 19, when nonlinear terms are included in the analysis. Thus, above $\mu = 0.3$, the introduction of moderate deflections or geometric nonlinearities is strongly destabilizing for a stiff-in-plane blade. This stability loss is associated with the change in the sign of various structural coupling terms obtained by going from a soft-in-plane design to a stiff-in-plane one*. The second lag mode was found to be stable for $0.0 < \mu < 0.40$, although it did exhibit a mild deterioration in stability up to $\mu = 0.2$, and only thereafter did it show an increase in stability. Also, the effect of nonlinear terms on this mode was not significant, this is illustrated in Fig. 20.

The stability variation of the flap and torsion modes is shown in Figs. 21 and 22 respectively. Clearly nonlinearities have a strong effect on both these degrees of freedom for this stiff-in-plane design. The first torsional mode is particularly sensitive to nonlinear terms. This is due to the numerous coupling terms in the torsion equation.

From Figs. 19-22 it is evident that nonlinear terms are destablizing for the fundamental lag mode and the first two flap modes; however, they are stabilizing for the first torsional mode. Since these nonlinearities can be both stabilizing and destablizing, this implies that nonlinear analyses based on moderate deflections are essential in order to reliably predict blade stability.

As mentioned previously, blade aeroelastic behavior is strongly dependent on the trim state. Results illustrating the difference between blade behavior for the propulsive and moment trim states are given in Ref. 25.

Additional results[25], not presented here, indicate that the reduction of aeroelastic stability margins evident for stiff in plane configurations is not apparent for soft-in-plane configurations. This tends to support the, known, superior aeroelastic characteristics of soft-in-plane configurations, when compared to stiff-in-plane blade configurations.

A number of previous analyses have considered the coupled flap-lag problem in forward flight[1,62,95]. Therefore, it is interesting to compare the results from the present coupled flap-lag-torsional analysis with a coupled flap-lag analysis in forward flight which is based on identical assumptions[86]. Such a comparison is presented in Fig. 23 for a soft-in-plane configuration under propulsive trim conditions with $C_W = 0.005$. The label CFLT on the curves denotes the results from the coupled flap-lag-torsional analysis. The comparison of real parts of the characteristic exponents for the first lag mode is

*See Ref. 25.

shown in Fig. 23. It is clear that the stability margin predicted for this mode from the flap-lag analysis is between 250-300% lower than the one predicted by the more accurate coupled flap-lag-torsional analysis. Since the stability margins predicted by the flap-lag analyses are low, these margins can easily show exagerated sensitivity to a variety of effects. It should be recognized that this sensitivity can be artificial, because it may be caused by the low damping levels predicted by the flap-lag analysis. Therefore, conclusions drawn from such analyses might be inaccurate[25].

The results presented in Figs. 19 through 23 were based on quasisteady aerodynamics in forward flight. Therefore, it is interesting to consider the influence of approximating some unsteady aerodynamic effects by using the dynamic inflow model[62]. The effect of dynamic inflow on coupled flap-lag motion in forward flight is shown in Figs. 24 and 25, which were taken from Ref. 62. These results were obtained for a three bladed rotor with $\bar{\omega}_{F1} = 1.15$; $R_c = 0$; $\gamma = 5.0$; $C_T = 0.01$; $\sigma = 0.05$; $C_{do} = 0.01$, pitch flap coupling parameter $\theta_\beta = 0$ and pitch lag coupling parameter $\theta_\zeta = 0$. These results were obtained using a moment trim procedure in forward flight. Blade stability is calculated from a linearized periodic system, using Floquet theory. The curves in the figures are labeled either no dynamic inflow or dynamic inflow. "No dynamic inflow" refers to the case in which induced flow perturbations are not accounted for, "dynamic inflow" refers to momentum theory with the apparent mass terms.

Figure 24 depicts the results for the effect of dynamic inflow on lead-lag damping of a stiff-in-plane rotor blade. The quantity η represents the real part of the characteristic exponent, identical to ζ_k in Eq. (31), plotted versus the advance ratio μ. The quantity ω_ζ is the collective lag frequency also denoted by $\bar{\omega}_{L1}$ in this paper. The collective and progressing modes show similar effects of dynamic inflow. As shown regressing mode $\omega = \omega_\zeta - 1 = 0.4$ is most affected by dynamic inflow. Dynamic inflow for this case is strongly stabilizing. The collective lag mode $\omega = \omega_\zeta$ and the progressing lag mode $\omega = \omega_\zeta + 1 = 2.4$ are affected to a lesser extent. Figure 25 shows the effect of dynamic inflow for a soft-in-plane blade. Again, the progressive, $\omega = \omega_\zeta + 1 = 1.7$, and collective branches, $\omega = \omega_\zeta = 0.7$, are rather close to each other. The frequencies of these modes (1.7 and 0.7) are much lower than those of the stiff-in-plane blade, and the total effect of dynamic inflow is therefore larger for $\omega_\zeta = 0.7$ than for $\omega_\zeta = 1.4$. The frequency of the regressing mode, $\omega = 1 - \omega_\zeta = 0.3$, is about the same for $\omega_\zeta = 0.7$ as it is for $\omega_\zeta = 1.4$ (0.3 versus 0.4). Therefore, the increase in percent critical damping is the same in either case (about 1%).

In interpreting the precise physical meaning of the results shown in Figures 24 and 25 a number of additional factors, due to some of the restrictive assumptions made in the calculations, should also be mentioned. Foremost is the assumption that the elastic coupling parameter $R_c = 0$, this assumption is somewhat unrealistic, particularly in presence of moment trim, since the elastic coupling terms[1] affect the blade by virtue of the cyclic pitch terms. Furthermore it is well known[1] that the flap-lag instability in hover is a mild instability which is completely eliminated in many cases by introducing elastic coupling.

It has been also indicated in the discussion of the results presented in Fig. 23, that flap-lag analyses can predict substantially lower levels of damping when compared to coupled flap-lag-torsional analyses. Low damping levels tend to overemphasize the importance of terms influencing damping, thus there

is a possibility that the magnitude of the dynamic inflow effects presented could be exagerated.

Figure 25 also shows that for the case of hover, $\mu = 0$, the difference due to dynamic inflow between the collective modes is approximately 20%. It is interesting to compare this result with the differences observed in the flap-lag branches of the stability boundary shown in Fig. 8, where Theodorsen type aerodynamics are compared to a quasi-steady aerodynamic theory in which the apparent mass terms have been neglected. The differences between the two curves are roughly of the same order of magnitude. Therefore, for the collective modes, the main source of difference between the results with dynamic inflow and those calculated without dynamic inflow might be attributed to apparent mass effects. Furthermore, it is difficult to compare Refs. 25 and 62 because the linearization used in Ref. 62, is not described in the paper.

Another important unsteady aerodynamic effect in forward flight is dynamic stall, which was not included in the results presented previously in this paper. Figure 26, taken from Ref. 72, illustrates the importance of this effect. The results presented in Fig. 25 are based upon the dynamic stall model which has been described in Section 2.4.2. This model was incorporated in a general computer module that computes rotor blade unsteady airloads[72]. The module also accounts for the fact that the blade section undergoes time varying changes in aerodynamic sweep angle and Mach number. Figure 26 presents the correlation between flight test data and the results of the G400 Aeroelastic Analysis, which is based upon Ref. 42, and utilizes the dynamic stall module[72]. The tests were carried out on a CH-53A aircraft. The predicted results are in good agreement with the test data when the blade is on the retreating side and undergoes dynamic stall. The onset of stall flutter is predicted reasonably well as indicated by the correlation of the results for the blade root torsion moment. The root torsion moment results also imply that the rotor blade leaves the stall flutter region at a later instant than predicted by the analysis. This may be attributed to the fact that the unsteady aerodynamic prediction method models the reattachment earlier than indicated by the test results. Normally, reattachment occurs at a lower angle than the static stall angle. In assessing the quality of the agreement between theory and test, which is evident from Fig. 26, it is important to note that accurate prediction of such loads is difficult to achieve[48].

Finally, it should be noted that the effect of more sophisticated aerodynamic models, including the influence of the wake and blade vortex interactions, on the flapping response of a rotor in hover and at low advance ratios has been presented in a recent paper by Johnson[111].

4. Formulation and Solution of Coupled Rotor/Fuselage Aeroelastic Problems

4.1 General

Analyses capable of modeling coupled rotor/fuselage aeroelastic systems have become increasingly important in recent years following the advent of hingeless rotored helicopters. Articulated rotors experienced mostly the classical ground resonance problem[4] which is a purely mechanical instability and represents a restricted class of problems where coupling between rotor and the fuselage can be simply represented and the effects of aerodynamics can be ignored. A study by Hammond[112] is representative of the more modern approach to this problem, another recent study of this mechanical instability has been performed by Bellavita et al[113].

Soft-in-plane hingeless rotor helicopters are susceptible to aeromechanical instabilities on the ground as well as in hover and forward flight. Instabilities of this type occur when the rotor lead-lag regressing mode and a body pitch or roll mode become proximate or coalesce. For the hingeless rotor helicopters coupling between the rotor and body is quite complex, and the rotor aerodynamics can significantly affect system stability[114,115]. The first detailed review of air resonance problems in hingeless rotor helicopters was carried out by Hohenemser[114]. Additional discussion of air and ground resonance problems is also available in Ref. 4. Coupled rotor fuselage analyses are also briefly reviewed in Ref. 1 and 116.

4.2 Formulation of Coupled Rotor/Fuselage Aeroelastic Problems

Formulation of coupled rotor/fuselage equations, intended for modeling the configuration shown in Fig. 27, is similar in many respects, to the isolated blade problem, which has been treated in Section 2. However, a number of substantial differences exist: (1) the equations are complicated by numerous additional terms associated with the motions of the fusealge. These terms contribute, significantly, to the algebraic complexity of the inertia and aerodynamic loads, (2) a modified form of the ordering scheme has to be used to restrict the equations to manageable size, and (3) rotor/fuselage coupling has to be performed in a careful systematic manner.

A number of recent models containing well documented formulations of coupled rotor/fuselage equations are available. Hodges [46] has developed a comprehensive model, including geometrical nonlinearities, which is suitable for modeling the aeromechanical stability of both bearingless and hingeless rotors in hover[44,45,115]. Warmbrodt and Friedmann[116] have derived the governing equations of motion of a helicopter rotor coupled to a rigid body fuselage. A reasonably consistent formulation is used to derive nonlinear periodic coefficient equations of motion which can be used to study coupled rotor/fuselage dynamics in forward flight. The methodology of rotor/fuselage coupling is clearly described and the importance of an ordering scheme in deriving consistent nonlinear equations of motion is reviewed. The final equations which are presented in partial differential form can be used to model aeroelastic stability or response of an N-bladed hingeless rotor (with each blade having flap-lag and torsional degrees of freedom).

Johnson[21,22,117] has developed a comprehensive analysis for rotorcraft which is capable of modeling coupled rotor/fuselage problems such as ground resonance, air resonance in hover and forward flight, in addition to a number of other aerodynamic and dynamic problems[21,22]. This model has been used quite successfully for hingeless rotor ground resonance prediction[22].

A recent detailed derivation of the air resonance problem in hover, of an N-bladed hingeless rotor helicopter has been presented by Levin[118]. In this study the final equations of dynamic equilibrium have been reduced to ordinary differential form by using Galerkin's method with a relatively small number of rotating blade modes. Provision for introducing active control of the rotor with the intent of eliminating the air resonance instability is included in the formulation.

The process of formulation of coupled rotor/fuselage aeroelastic problems can be illustrated with a sufficient degree of clarity only by following a specific example. The example selected for this purpose is Ref. 118, which

is restricted to the case of hover. A very similar derivation representing a generalization of this formulation to forward flight is also available[116].

The most important assumptions upon which the formulation is based are: (1) the helicopter is in hover with low disc loading (low inflow ratio), (2) the rigid fuselage has two translational degrees of freedom and two rotational degrees of freedom; vertical translation and rotation about the vertical axis (yawing) are eliminated, (3) the rotor consists of three or more hingeless blades, (4) each blade can bend in two mutually perpendicular direction normal to the elastic axis and can twist torsionally about the elastic axis. Elastic deformations are moderate resulting in finite rotations but small strains. Additional assumptions can be found in Ref 118 and 116. The geometry of the problem is shown in Fig. 27.

Structural Modeling of the blades is identical to the description presented in Section 2.2 and is based on the transformation given by Eq. (1).

Inertia Modeling for coupled rotor/fuselage problem is more complicated than for the isolated blade problems. Since the hub, or center of rotation is also moving due to fuselage translation and rotation, the absolute acceleration of a mass point in the cross section of the k^{th} blade is given by[119]

$$\bar{a}_{pk} = \ddot{\bar{R}}_o + \ddot{\bar{r}}_{pk} + 2\bar{\omega}_k \times \dot{\bar{r}}_{pk} + \dot{\bar{\omega}}_k \times \bar{r}_{pk} + \bar{\omega}_k \times (\bar{\omega}_k \times \bar{r}_{pk}) \tag{33}$$

and the angular velocity is

$$\bar{\omega}_k = \bar{\omega}_F + \Omega \bar{e}_{1z} \tag{34}$$

where $\bar{R}_o$ is the position vector of the moving coordinate system with respect to the inertial, $\bar{r}_{pk}$ is the position vector of the point P in the k^{th} blade from the origin of the moving reference frame and $\bar{\omega}_k$ is the angular velocity of the moving coordinate system.

Furthermore, in addition to the blade inertia loads, the fuselage inertia loads, due to the fuselage motions are also required. The details for deriving these inertia loads can be found in Ref. 118.

When geometric nonlinearity is incorporated in the blade equations, blade inertia loads contain numerous additional small terms due to fuselage dynamics.

Aerodynamic Modeling of coupled rotor fuselage problems is similar to the discussion presented for the isolated blade case in Section 2.4. The algebraic complexity of the formulation increases substantially due to the presence of numerous small terms, associated with fuselage dynamics, in the relative velocity components at the deformed blade cross section[116,118]. Therefore, these is a general tendency to use simple aerodynamic models, such as quasi-steady aerodynamics, which was used in Ref. 116 and 118. For coupled rotor/fuselage problems unsteady aerodynamic effects can be approximated, reasonably, by introducing dynamic inflow, as described by Eq. (9).

Ordering Schemes for coupled rotor/fuselage equations of motion are very important since incorporation of moderate blade deflections gives rise to a plethora of higher order terms. It is practically impossible to retain all higher order terms, hence a large quantity of small higher order terms are usually neglected. Identification of higher order terms in a rational and systematic manner is accomplished by using an ordering scheme similar to the one discussed in Section 2.5. The order of magnitude assigned to fuselage motions has a drastic effect on the number of terms retained in the analysis. The selection of the appropriate order of magnitude for fuselage motion is constrained by two conflicting requirements: on one hand the orders of magnitude of fuselage motion must not be so small as to eliminate physically significant coupling effects from the governing equations, on the other hand the number of terms retained should be manageable from an algebraic manipulative point of view. Taking these conflicting considerations into account the fuselage motions are assigned to be[118]

$$\frac{R_x}{R} \ , \ \frac{R_y}{R} \ , \ \frac{R_z}{R} \ , \ \theta_x, \theta_y, \theta_z = O(\varepsilon^{3/2})$$

With these orders of magnitude, the important coupling effects are retained, while certain higher order coupling effects, such as those which induce propeller-whirl flutter are lost. Were the higher order effects required, $O(\varepsilon)$ insteady of $O(\varepsilon^{3/2})$ for fuselage motions would be needed. Additional useful considerations regarding the orders of magnitude of various quantities, can be found in Ref. 118.

Coordinate Systems are central to the derivation of the nonlinear blade equations and the matching of rotor forces, moments and displacements at the rotor hub with those of the fuselage. The definition of the precise relationship between the various cartesian coordinate system is required, in form of numerous coordinate transformations. In the formulation presented by Levin[118] seven different coordinate systems have been utilized, requiring a considerable amount of "book-keeping". Similar coordinate systems are also used in Ref. 116.

Matching Conditions at the Rotor Hub are obtained by enforcing dynamic equilibrium of the forces $\bar{P}$ and the moments $\bar{Q}$ at the hub. For this particular example, these conditions are

$$\begin{aligned} P_{HX} + P_{GFX} + P_{RX} + P_{GRX} + 0 \\ P_{HY} + P_{GFY} + P_{RY} + P_{GRY} = 0 \\ Q_{HX} + Q_{GFY} + Q_{RX} = 0 \\ Q_{HY} + Q_{GFY} + Q_{RY} = 0 \end{aligned} \tag{35}$$

where P_{HX}, P_{HY}, Q_{HX}, Q_{HY} are the appropriate components of the fuselage inertial force and moment vectors; P_{GFX}, P_{GFY}, Q_{GFX}, Q_{GFY} are the appropriate components of the fuselage gravitational force and moment vectors; P_{RX}, P_{RY}, Q_{RX}, Q_{RY} are the appropriate components of the rotor load force and moment vectors due to inertial, aerodynamic and structural damping loads in the blades; P_{GRX} and P_{GRY} are the appropriate components of the gravitational force vector on the rotor.

The rotor load force and moment vectors are obtained by performing a summation over the individual blades

$$\bar{P}_R = \sum_{k=1}^{N} \bar{P}_{Rk}$$

$$\bar{Q}_R = \sum_{k=1}^{N} \bar{Q}_{Rk} \tag{36}$$

Furthermore, the quantity x_F, shown in Fig. 27, was taken as $x_F = 0$[118]. This procedure leads to a total of $3N + 4$ dynamic equations of equilibrium for this coupled rotor/fuselage system.

4.3 Solution of Coupled Rotor/Fuselage Aeroelastic Problems

The solution of coupled rotor/fuselage problems follows essentially the procedures outlined in Section 3[118]. The first step is the spatial discretization of the blade equations of motion using Galerkin's method based on the uncoupled first rotating modes for each of the flap, lag and torsion elastic degrees of freedom for a cantilevered beam. Thus the modal substitutions, corresponding to Eqs. (13), are

$$\begin{aligned} w_k &= \ell g_k(\psi)\eta(\bar{x}_o) \\ v_k &= -\ell h_k(\psi)\gamma(\bar{x}_o) \\ \phi_k &= f_k(\psi)\phi(\bar{x}_o) \end{aligned} \tag{37}$$

Thus, the partial differential equations are transformed into a set of nonlinear ordinary differential equations with periodic coefficients, for the k^{th} blade. For the case of hover the equations which define the static equilibrium of the blade are found by requiring that all time derivatives and fuselage perturbations vanish in the equations. Thus the static equilibrium state is identical for all N-blades. This static equilibrium condition can be obtained using the method described in Section 3.2.2.

Next, the amplitudes of the k^{th} blade's modes (or generalized coordinates) are expressed as time varying perturbations about the static equilibrium values, g_o, h_o and f_o respectively

$$\begin{aligned} g_k(\psi) &= g_o + \Delta g_k(\psi) \\ h_k(\psi) &= h_o + \Delta h_k(\psi) \\ f_k(\psi) &= f_o + \Delta f_k(\psi) \end{aligned} \tag{38}$$

and linearized perturbation equations are obtained. The linearized perturbation equations of the k^{th} blade have periodic coefficients, since they are written in a blade fixed coordinate system. Transformation of the perturbation equations to the hub fixed, rotor plane coordinate system[118] will result in perturbation equations with constant coefficients. It should be noted that rotor-plane coordinates are variously referred to as Coleman coordinates or multiblade coordinates[100], and Fourier coordinates[4]. It is felt that the designation "rotor-plane coordinates" more accurately conveys the salient characteristics of these coordinates than do other designations[118].

The stability of the system of 3N + 4 linearized, constant coefficient equations can be solved by using conventional eigenanalysis, as indicated in Section 3.2.2. Hodges has used an approach identical, to the one outlined above, for solving the aeromechanical stability problem of bearingless rotors [44,45].

For the case of forward flight, transformation to rotor-plane (or multiblade) coordinates will not remove all periodic coefficients. Under these conditions, the blade equations can be used in their original blade fixed formulation, and solutions can be obtained using the approach outlined in Section 3.2.3. This approach was successfully used[120] for studying the coupled rotor/tower dynamics of large horizontal axis wind turbines, which is mathematically similar to the coupled rotor/fuselage problem in forward flight.

4.4 Coupled Rotor/Fuselage, Some Illustrative Results

The material presented in this section is intended to augment the theoretical material of the previous sections. Hodges has conducted a theoretical study of the aeromechanical stability of bearingless rotors in hover[45] by comparing the hub-fixed motion, i.e. isolated blade stability, with the case when coupled rotor-body motion is considered. His studies dealt mostly with soft-in-plane configurations using quasisteady aerodynamics. He concluded that system parameters can be chosen to stabilize most soft-in-plane configurations for the hub fixed case. Under certain conditions the same parameters can also stabilize the coupled rotor-body system in hovering flight, i.e in air resonance. However, when the rotorcraft is in contact with the ground and near zero thrust, it appeared that these parameters are not as effective in stabilizing the system in the ground resonance mode. He has also compared his analytical results with experimental data on bearingless main rotors and obtained good correlation[44]. Hodges analytical model was also used to study hingeless rotor aeromechanical stability by comparing the theory with experimental data obtained by Bousman[115]. The overall agreement between experimental data and theoretical predictions was good.

More recently Bousman conducted a careful experimental investigation of the effects of aeroelastic couplings on the aeromechanical stability of a hingeless rotor helicopter[121]. Five different configurations were tested, to determine to what extent, pitch-lag coupling and structural coupling can successfully stabilize the air resonance mode. The experimental results were also compared with Hodges[44,45] theoretical model. The measured lead-lag regressing mode damping agreed well with theory. Comparison of theory and experiment for the damping of the body modes showed significant differences which were attributed by Bousman to rotor inflow dynamics.

Recently, Johnson[22,122] compared Bousman's[121] results with analytical predictions of ground resonance, using the model described in Ref. 117. The calculations were performed with and without dynamic inflow, using a model similar, to the dynamic inflow represented by Eq. (9). The experiments[121] were conducted on a three bladed rotor which had a radius R = 0.811m, a solidity 0.0494, and a Lock number of $\gamma = 6.1$. For the cases considered here, the untwisted blades were operated at zero pitch of the structural axes. The blades had flap and lag flexures at radial station 0.105. The gimbal pitch and roll spring rates were such that resonances of the body modes with the regressing lag mode occurred where the lag frequency was below once-per-revolution. Hence a ground resonance instability was possible, depending on system damping. The blade flap flexure produced a rotating natural frequency of $\bar{\omega}_{F1} = 1.12$ at high

rotor speed. The rotating natural frequency of the lag mode was $\bar{\omega}_{L1} = 0.81$ at the body pitch mode resonance (585 RPM), and $\bar{\omega}_{L1} = 0.69$ at the body roll mode resonance (745 RPM). In the analysis only fundamental flap and lag modes were considered. Higher bending modes and torsion were neglected[22,122]. The degrees of freedom used in the flutter analysis were the flap and lag motion and the rotor inflow dynamics variables. The conning, collective lag, and uniform inflow degrees of freedom form a separate set, that decouples from the ground resonance problem in hover.

The damping in the regressing lag mode, body pitch mode and body roll mode as a function of the rotor speed is presented in Figs. 28 to 30. The eigenvalues are $\sigma \pm \omega$, where ω is the frequency and σ is the damping. The blade and body mode damping is predicted well although smaller values of system structural damping would improve the correlation for the lag mode at the instability. The calculated damping is in error without the inflow dynamics. In particular, the body roll mode damping is greatly overpredicted at high rotor speed as shown in Fig. 30.

In a different study, Kato et al[123] have found that using Loewy's unsteady aerodynamic theory improves agreement between theory and test. The objective of this study was to determine the vertical impedance of a hovering rotor. Thus it appears that the use of theories having even a limited degree of unsteady aerodynamic modeling capability are preferable to quasi-steady models for coupled rotor/fuselage analyses.

Another recent study by Gaonkar et al[124] has considered the sensitivity of helicopter aeromechanical stability to dynamic inflow using a purely theoretical approach. The results do indicate that dynamic inflow can influence both air and ground resonance. Since the regressing lag role plays an important role in air and ground resonance problems, the sensitivity exhibited, reflects upon the influence of dynamic inflow on this mode, which was treated previously in detail[62].

It is also important to note that body roll mode damping reduction, due to dynamic inflow, shown in Fig. 30 was also noted in the results presented in Ref. 124. Clearly, this also implies that a better representation of unsteady aerodynamics is important in coupled rotor/body problems involving hingeless rotor configurations. Because the cantilever restraint of blade flap motion allows the rotor to develop net pitch and roll moments which in turn cause induced velocity perturbations, which are equivalent to a low frequency unsteady aerodynamic effect.

5. Concluding Remarks

The broad spectrum of activity described in the paper indicates that rotary-wing aeroelasticity is one of the most active and challenging areas of modern aeroelasticity. Recent research has clarified a number of fundamental problems. Treatment of geometrical nonlinearities has become routine for bearingless and hingeless rotors. Geometrical nonlinearities have proven to be important for establishing aeroelastic stability boundaries in both hover and in forward flight. It is also apparent that these nonlinearities can also effect response calculations, although their importance is smaller than for stability calculations. Modern semiempirical dynamic stall models show significant potential towards simulating blade loads and response at high advance ratios. A fundamental understanding of coupled rotor/fuselage problems has emerged. Furthermore, the carefully established data base for coupled rotor/fuselage

aeromechanical problems will serve as an extremely useful base for validating more elaborate analyses. Advances have been made in the mathematical treatment of equations with periodic coefficient, these will serve as a useful tool for aeroelastic analyses in forward flight.

However, much remains to be done. Better unsteady aerodynamic models, simulating forward flight, compressibility and trasonic effects have to be developed. These unsteady aerodynamic theories, should be compatible with the coupled flap-lag-torsional dynamics of the rotor blade and should be suitable for incorporation in aeroelastic analyses. Finally, the existing experimental data base for hover should be also extended to the forward flight regime.

References

1. Friedmann, P.P., Recent developments in rotary-wing aeroelasticity, Journal of Aircraft, Vol. 14, No. 11, November 1977, pp. 1027-1041.

2. Bramwell, A.R.S., Helicopter dynamics, John Wiley & Sons, 1976.

3. Dowell, E H., et al, A modern course in aeroelasticity, Sijthoff & Noordhoff, 1978.

4. Johnson, W., Helicopter theory, Princeton University Press, 1980.

5. Jenney, D.S., ABC aircraft development status, Paper No. 8, Proceedings Six European Rotorcraft and Powered Lift Aircraft Forum, Bristol, England, September 1980, pp. 8.1-8.16.

6. Linden, A. and Ruddell, A., An ABC status report, Proceedings of the 37th Annual Forum of the American Helicopter Society, New Orleans, May 1981, pp. 72-87.

7. Bilger, J.M., Mar, R.L., and Zahedi, A., Results of the structural dynamic testing of the XV-15 tilt rotor research aircraft, Proceedings of the 37th Annual Forum of the American Helicopter Society, New Orleans, May 1981, pp. 493-502.

8. Williams, R.M., Application of circulation control rotor technology to a stopped rotor aircraft design, Vertica, Vol. 1, No. 1, 1976, pp. 3-15.

9. Potthast, A.J., X-wing stability and control development and wind tunnel demonstration tests - helicopter, conversion and fixed wing flight, Paper No. 80-27, 36th Annual Forum of the American Helicopter Society, Washington, D.C., May 1980.

10. Dixon, P.G.C., Design, development, and flight demonstration of the loads and stability characteristics of a bearingless main rotor, USA AVRADCOM-TR-80-D-3, June 1980.

11. Staley, J.A., Gabel, R , and McDonald, H.I., Full scale ground and air resonance testing of the army-boeing vertol bearingless main rotor, Paper No. 79-23, Proceedings of the 35th Annual National Forum of the American Helicopter Society, May 1979.

12. Warmbrodt, W., McCloud, J., III, Sheffler, M. and Staley, J.A., Full-scale wind tunnel test of the aeroelastic stability of a bearingless main rotor, Proceedings of the 37th Annual Forum of the American Helicopter Society, New Orleans, May 1981, pp. 204-216.

13. Fenaughty, R.R. and Noehren, W L., Composite bearingless tail rotor for UTTAS, Journal of the American Helicopter Society, Vol. 22, No. 3, July 1977, pp. 19-26.

14. Shaw, J. and Edwards, W.T., The YUH-61A tail rotor: development of a stiff inplane bearingless flexstrap design, Journal of the American Helicopter Society, Vol. 23, No. 2, April 1978, pp. 9-18.

15. Huber, H., Frommlet, H. and Buchs, W., Development of a bearingless helicopter tail-rotor, Vertica - The International Journal of Rotorcraft and Powered Lift Aircraft, Vol. 5, No. 2, 1981, pp. 131-147.

16. Cresap, W.L., Myers, A W. and Viswanathan, S.P., Design and development tests of a four-bladed light helicopter rotor system, Journal of the American Helicopter Society, Vol. 24, No 1, January 1979, pp. 20-25.

17. Viswanathan, S.P., and Myers, A.W., Reduction of helicopter vibration through control of hub-impedance, Journal of the American Helicopter Society, Vol. 25, No. 4, October 1980, pp. 3-12.

18. Cassier, A., Development of the triflex rotor head, Journal of the American Helicopter Society, Vol. 26, No. 3, July 1981, pp. 25-31.

19. Reddy, D.J., Qualification program of the composite main rotor blade for the model 214B helicopter, Journal of the American Helicopter Society, Vol. 25, No. 3, July 1980, pp. 10-14.

20. Wehnert, G.J., Sheffler, M.W. and Reddick, H.K., Boeing vertol bearingless main rotor structural design approach using advanced composites, Preprint No. 19, AHS/NASA-Ames Conference on Helicopter Structural Technology, November 1977.

21. Johnson, W., Development of a comprehensive analysis for rotorcraft, part I: rotor model and wake analysis, Vertica - The International Journal of Rotorcraft and Powered Lift Aircraft, Vol. 5, No. 2, 1981, pp. 99-129.

22. Johnson, W., Development of a comprehensive analysis for rotorcraft, part II: aircraft model, solution procedure and applications, Vertica - The International Journal of Rotorcraft and Powered Lift Aircraft, Vol. 5, No. 3, 1981, pp. 185-216.

23. Anon., Workshop on unified equations for rotorcraft systems modeling, Aeromechanics Laboratory, AVRADCOM, NASA Ames Research Center, Moffett Field, California, February 1979.

24. Hodges, D.H. and Ormiston, R.A., Stability of elastic bending and torsion of uniform cantilever rotor blades in hover with variable structural coupling, NASA TN D-8192, 1976.

25. Friedmann, P.P. and Kottapalli, S.B.R., Rotor blade aeroelastic stability and response in forward flight, Paper No. 14, Proceedings of Sixth European Rotorcraft and Powered Lift Aircraft Forum, September 1980, pp. 14.1-14.34.

26. Reichert, G., Helicopter vibration control - a survey, Vertica - The International Journal of Rotorcraft and Powered Lift Aircraft, Vol. 5, No. 1, 1981, pp. 1-20.

27. Johnson, W., Self-tuning regulators for multicylic control of helicopter vibration, NASA TP-1996, March 1982.

28. Rosen, A. and Friedmann, P., Nonlinear equations of equilibrium for elastic helicopter or wind turbine blades undergoing moderate deformation, University of California, Los Angeles, School of Engineering and Applied Science Report, UCLA-ENG-7718, Revised Ed. June 1977 (also available as NASA CR-159478, December 1978.

29. Shamie, J. and Friedmann, P., Effect of moderate deflections on the aeroelastic stability of a rotor blade in forward flight, Paper No. 24, Proceedings of Third European Rotorcraft and Powered Lift Aircraft Forum, Aix-en-Provence, France, September 1977, pp. 24.1-24.37.

30. Kaza, K.R. and Kvaternik, R G., Nonlinear aeroelastic equations for combined flapwise bending, chordwise bending, torsion, and extension of twisted nonuniform rotor blades in forward flight, NASA Technical Memorandum 74059, August 1977.

31. Hodges, D.H., Ormiston, R A. and Peters, D.A., On the nonlinear deformation geometry of Euler-Bernoulli beams, NASA Technical Paper 1566, April 1980.

32. Dowell, E.H., Traybar, J. and Hodges, D.H., An experimental theoretical correlation study of non-linear bending and torsion deformations of a cantilever beam, Journal of Sound and Vibration, Vol. 50, No. 4, 1977, pp. 533-544.

33. Rosen, A. and Friedmann, P., The nonlinear behavior of elastic slender straight beams undergoing small strains and moderate rotations, ASME Journal of Applied Mechanics, Vol. 46, March 1979, pp. 161-168.

34. Houbolt, J.C. and Brooks, G.W., Differential equations of motion for combined flapwise bending, chordwise bending and torsion of twisted nonuniform rotor blades, NACA Report 1346, 1958.

35. Rosen, A., The effect of initial twist on the torsional rigidity of beams - Another point of view, ASME - Journal of Applied Mechanics, Vol. 47, June 1980, pp. 389-393.

36. Hodges, D.H., Torsion of pretwisted beams due to axial loading, ASME - Journal of Applied Mechanics, Vol. 47, June 1980, pp. 393-397.

37. Petersen, D., Interaction of torsion and tension in beam theory, Paper No. 20, Proceedings of Sixth European Rotorcraft and Powered Lift Aircraft Forum, Bristol, England, September 1980.

38. Stephen, N.G. and Levinson, M., A second order beam theroy, Journal of Sound and Vibration, Vol. 67, No. 3, 1979, pp. 293-305.

39. Rehfield, L.W. and Murthy, L.N.P., Toward a new engineering theory of bending, AIAA Paper 80-0683-CP, 21st AIAA/ASME/ASCE/AHS, Structures, Structural Dynamics and Materials Conference, Seattle, Wa., May 1980.

40. Worndle, R., Calculation of the cross section properties and the shear stresses of composite rotor blades, Paper No. 65, Proceedings of the Seventh European Rotorcraft and Powered Lift Aircraft Forum, Garmisch-Partenkirchen, Federal Republic of Germany, September 1981.

41. Bielawa, R.L., Cheney, Jr., M.C. and Novak, R.C., Investigation of a bearingless helicopter rotor concept having a composite primary structure, NASA CR-2637, 1976.

42. Bielawa, R.L., Aeroelastic analysis for helicopter rotor blades with time variable, nonlinear structural twist and multiple structural redundance - mathematical derivation and program user's manual, NASA CR-2638, 1976.

43. Harvey, K.W., Aeroelastic analysis of a bearingless rotor, American Helicopter Society Symposium on Rotor Technology, Essington, Pa., August 1976.

44. Hodges, D.H., An aeromechanical stability analysis for bearingless rotor helicopters, Journal of the American Helicopter Society, Vol. 24, No. 1, January 1979, pp. 2-9.

45. Hodges, D.H., A theoretical technique for analyzing the aeroelastic stability of bearingless rotors, AIAA Journal, Vol. 17, No. 4, April 1979, pp. 400-407.

46. Hodges, D.H., Aeromechanical stability of helicopters with a bearingless main rotor - part I: equations of motion, NASA TM-78459, 1978.

47. Ormiston, R.A. and Bousman, W.G., A study of stall induced flap-lag instability of hingeless rotors, Journal of the American Helicopter Society, Vol. 20, No. 1, January 1975, pp. 20-30.

48. Ormiston, R.A., Comparison of several methods for predicting loads on a hypothetical helicopter rotor, Journal of the American Helicopter Society, Vol. 19, No. 4, October 1974, pp. 2-13.

49. Bisplinghoff, R.L., Ashley, H., and Halfman, R.L., Aeroelasticity, Addison-Wesley Inc., 1955 (p. 272).

50. Ham, N.D., Helicopter blade flutter, Agard Rep. 607, 1973 (revision of Part III, Chap. 10 of the Agard Manual on Aeroelasticity).

51. Friedmann, P. and Yuan, C., Effect of modified aerodynamic strip theories on rotor blade aeroelastic stability, AIAA Journal, Vol. 15, No. 7, July 1977, pp. 932-940.

52. Greenberg, J.M., Airfoil in sinusoidal motion in a pulsating stream, NACA TN 1326, 1947.

53. Johnson, W., Application of unsteady airfoil theory to rotary wings, Journal of Aircraft, Vol. 17, No. 4, April 1980, pp. 285-286.

54. Kaza, K.R.V. and Kvaternik, R.G., Application of unsteady airfoil theory to rotary wings, Journal of Aircraft, Vol. 18, No. 7, July 1981, pp. 604-605.

55. Kottapalli, S.B.R. and Pierce, G.A., Drag on an oscillating airfoil in a fluctuating free stream, ASME Journal of Fluids Engineering, Vol. 101, September 1979, pp. 391-399.

56. Kottapalli, S.B.R., Drag on an oscillating airfoil in a fluctuating free stream, Ph.D. Dissertation, School of Aerospace Engineering, Georgia Institute of Technology, August 1977.

57. Loewy, R.G., A two dimensional approximation to the unsteady aerodynamics of rotary wings, Journal of the Aeronautical Sciences, Vol. 24, 1957, pp. 81-92, 144.

58. Yuan, C. and Friedmann P., A study of the effect of unsteady aerodynamics on the aeroelastic stability of rotor blades in hover, University of California, Los Angeles, School of Engineering and Applied Science, Report UCLA ENG-7721, February 1977.

59. Jones, W.P. and Rao, B.M., Compressibility effects on oscillating rotor blades in hovering flight, AIAA Journal, Vol. 8, No. 2, February 1979, pp. 321-329.

60. Hammond, C.E. and Pierce G.C., A compressible unsteady aerodynamic theory for helicopter rotors, AGARD Specialists Meeting on the Aerodynamics of Rotary Wings, Marseille, France, September 1972.

61. Jones, W.P., McCroskey, W.J. and Costes, J.J., Unsteady aerodynamics of helicopter rotors, AGARD Rep. No. 595, April 1972.

62. Peters, D.A. and Gaonkar, G.H., Theoretical flap-lag damping with various dynamic inflow models, Journal of the American Helicopter Society, Vol. 25, No. 3, July 1980, pp. 29-36.

63. Crews, S.T., Unsteady hovering rotor wake parameters identified from dynamic model tests, D.Sc Thesis, Washington University, St. Louis, Missouri, 1977.

64. Banerjee, D., Crews, S.T., Hohenemser, K.H., and Yin, S.K., Identification of state variables and dynamic inflow from rotor model dynamic tests, Journal of the American Helicopter Society, Vol. 22, No. 2, April 1977, pp. 28-36.

65. Banerjee, D., Crews, S.T. and Hohenemser, K.H., Parameter identification applied to analytic hingeless rotor modeling, Journal of the American Helicopter Society, Vol. 24, No. 1, January 1979, pp. 26-32.

66. Pit, D.M. and Peters, D.A., Theoretical prediction of dynamic inflow derivatives, Vertica - The International Journal of Rotorcraft and Powered Lift Aircraft, Vol. 5, No. 1, 1981, pp. 21-34.

67. Ormiston, R.A., An actuator disc theory for rotor wake induced velocities, AGARD Specialists' Meeting on the Aerodynamics of Rotary Wings, Marseilles, France, 1972.

68. Huber, H. and Mikulla, V., Transonic effects on helicopter rotor blades, Proceedings International Symposium on Aeroelasticity, Nuremberg, Federal Republic of Germany, October 5-7, 1981.

69. Huber, H. and Strehlow, H., Hingeless rotor dynamics in high speed flight, Vertica - The International Journal of Rotorcraft and Powered Lift Aircraft, Vol. 1, No. 1, 1976, pp. 39-53.

70. Caradonna, F.X. and Philippe, J.J., The flow over a helicopter blade tip in the transonic regime, Vertica - The International Journal of Rotorcraft and Powered Lift Aircraft, Vol. 2, No. 1, 1978, pp. 43-60.

71. Tauber, M.E. and Hicks, R.M., Computerized three-dimensional aerodynamic design of a lifting rotor blade, Paper No. 80-2, Proceedings 36th Annual Forum of the American Helicopter Society, Washington, D.C., May 1980.

72. Gangwani, S.T., Prediction of dynamic stall and unsteady airloads for rotor blades, Proceedings of 37th Annual Forum of the American Helicopter Society, New Orleans, May 1981, pp. 1-17.

73. McCroskey, W.J., Some current research in unsteady fluid dynamics - the 1976 Freeman Scholar lecture, ASME Journal of Fluids Engineering, Vol. 1, 1977, pp. 8-39.

74. Carr, L.W., McAllister, K.W. and McCroskey, W.J., Analysis of the development of dynamic stall based on oscillating airfoil experiments, NASA TN D-8283, January 1977.

75. McCroskey, W.J., McAllister, K.W., Carr, L.W., Pucci, S.L., Lambert, O., and Indergrand, R.F., Dynamic stall on advanced airfoil sections, Journal of the American Helicopter Society, Vol. 26, No. 3, July 1981, pp. 40-50.

76. Mehta, U.B., Dynamic stall of an oscillating airfoil, AGARD Conference Proceedings No. 227, Unsteady Aerodynamics, Fluid Dynamics Panel Symposium, Ottawa, Canada, September 1977, Paper No. 23, pp. 23.1-23.32.

77. Beddoes, T.S., A synthesis of unsteady aerodynamic effects including stall hysteresis, Vertica - The International Journal of Rotorcraft and Powered Lift Aircraft, Vol. 1, No. 2, 1976, pp. 113-123.

78. Dat, R., Tran, C.T. and Petot, D., Modele phenomenologique de decrochage dynamique sur profil de pale d'helicoptere, XVI Collogue d'Aerodynamique Appliquee (AAAF), Lille, November 1979.

79. Tran, C.T. and Petot, D., Semi-empirical model for the dynamic stall of airfoils in view of the application to the calculation of the responses of a helicopter blade in forward flight, Vertica, Vol. 5, No. 1, 1981, pp. 35-53.

80. Lawson, C.L. and Hanson, R.J., Solving least squares problems, Prentice-Hall Inc., 1974.

81. Pierce, G.A., Kunz, D.L. and Malone, J.B., The effect of varying freestream velocity on airfoil dynamic stall characteristics, Journal of the American Helicopter Society, Vol. 23, No. 2, April 1978, pp. 27-33.

82. Hodges, D.H. and Dowell, E.H., Nonlinear equations of motion for the elastic bending and torsion of twisted nonuniform rotor blades, NASA TN D-7818, 1974.

83. Friedmann, P., Influence of modeling and blade parameters on the aeroelastic stability of a cantilevered rotor, AIAA Journal, Vol. 15, No. 2, February 1977, pp. 149-158.

84. Hansford, R.E., Comparison of predicted and experimental loads to evaluate flap-lag coupling with blade pitch, Journal of the American Helicopter Society, Vol. 24, No. 5, October 1979, pp. 3-11.

85. Friedmann, P.P. and Straub, F., Application of the finite element method to rotary-wing aeroelasticity, Journal of the American Helicopter Society, Vol. 25, No. 1, January 1980, pp. 36-44.

86. Straub, F.K. and Friedmann, P.P., A Galerkin type finite element method for rotary-wing aeroelasticity in hover and forward flight, Vertica, Vol. 5, No. 1, 1981, pp. 75-98.

87. Sivaneri, N.T. and Chopra, I., Dynamic stability of a rotor blade using finite element analysis, Proceedings of AIAA/ASME/ASCE/AHS 22nd Structures, Structural Dynamics and Materials Conference and AIAA Dynamics Specialist Conference, CP 812, Part 1, Atlanta, Georgia, April 1981, pp. 832-843.

88. Straub, F.K., Application of the finite element method to rotary-wing aeroelasticity, Ph.D. Dissertation, Mechanics and Structures Department, University of California, Los Angeles, April 1980.

89. Hodges, D.H. and Rutkowski, M., Free-vibration analysis of rotating beams by a variable-order finite-element method, AIAA Journal, Vol. 19, No. 11, November 1981, pp. 1459-1466.

90. Hunter, W.F., The integrating matrix method for determining the natural vibration characteristics of propeller blades, NASA TN D-6064, December 1970.

91. White, W.F. and Malatino, R.E., A numerical method for determining the natural vibration characteristics of rotating nonuniform cantilever blades, NASA TMX-72751, October 1975.

92. Kvaternik, R.G., White, W.F., and Kaza, K.R., Nonlinear flap-lag-axial equations of a rotating beam with arbitrary precone angle, AIAA Paper 78-491, Proceedings of AIAA/ASME 19th Structures, Structural Dynamics and Materials Conference, Bethesda, Maryland, pp. 214-227, April 1978.

93. White W.F., Effect of compressibility on three-dimensional helicopter rotor blade flutter, Ph.D. Dissertation, Georgia Institute of Technology, School of Aerospace Engineering, March 1973.

94. Giurgiutiu, V., Vibrations and dynamic stability of rotor blades, Ph.D. Dissertation, Dept. of Aeronautics, Imperial College of Science and Technology, University of London, 1977.

95. Friedmann, P. and Shamie, J., Aeroelastic stability of trimmed helicopter blades in forward flight, Vertica, Vol. 1, No. 3, 1977, pp. 189-211.

96. Kottapalli, S.B.R., Friedmann, P.P. and Rosen, A., Aeroelastic stability and response of horizontal axis wind turbine blades, AIAA Journal, Vol. 17, No. 12, December 1979, pp. 1381-1389.

97. Peters, D.A. and Izadpanah, A.P., Helicopter trim by periodic shooting with Newton-Raphson iteration, Proceedings of the American Helicopter Society 37th Annual Forum, New Orleans, May 1981, pp. 217-226.

98. Friedmann, P., Hammond, C.E. and Woo, T., Efficient numerical treatment of periodic systems with application to stability problems, International Journal of Numerical Methods in Engineering, Vol. 11, 1977, pp. 1117-1136.

99. Gaonkar, G.H., Simha Prasad, D.S. and Sastry, D., On computing floquet transition matrices for rotorcraft, Journal of the American Helicopter Society, Vol. 26, No. 3, July 1981, pp. 56-61.

100. Hohenemser, K.H. and Yin, S.K., Some applications of the method of multiblade coordinates, Journal of the American Helicopter Society, Vol. 17, No. 3, July 1972, pp. 1-12.

101. Gaonkar, G.H. and Peters, D.A., Use of multiblade coordinates for helicopter flap-lag stability with dynamic inflow, Journal of Aircraft, Vol. 17, February 1980, pp. 112-118.

102. Biggers, J.C., Some approximations to the flapping stability of helicopter rotors, Journal of the American Helicopter Society, Vol. 14, No. 4, October 1974, pp. 24-33.

103. Prussing, J.E., Orthogonal multiblade coordinates, Journal of Aircraft, Vol. 18, No. 6, June 1981, pp. 504-506.

104. Dugundji, J. and Wendel, J.H., General review of the Mostas computer code for wind turbines, NASA CR-165385, June 1981.

105. Bathe, K.J. and Wilson, E.L., Numerical methods in finite element analysis, Prentice Hall, 1976, Ch. 8-9.

106. Gear, C.W., Numerical initial value problems in ordinary differential equations, Prentice Hall, 1971.

107. Hall, T.E., Enright, W.H., Fellen, B.M., and Sedgwick, A.E., Comparing numerical methods for ordinary differential equations, SIAM Journal of Numerical Analysis, Vol. 4, No. 2, December 1972, pp. 603-637.

108. Tran, C.T. and Falchero, D., Application of the ONERA dynamic stall model to a helicopter blade in forward flight, Paper No. 46, Proceedings of Seventh European Rotorcraft and Powered Lift Aircraft Forum, Garmisch-Partenkirchen, Germany, September 1981, pp. 46.1-46.25.

109. Hsu, C.S., On approximating a general linear periodic system, Journal of Mathematical Analysis and Applications, Vol. 45, 1974, pp. 234-251.

110. Friedmann, P. and Silverthorn, L.J., Aeroelastic stability of periodic systems with application to rotor blade flutter, AIAA Journal, Vol. 12, No. 11, November 1974, pp. 1559-1565.

111. Johnson, W., Comparison of calculated and measured helicopter rotor lateral flapping angles, Journal of the American Helicopter Society, Vol. 26, No. 2, April 1981, pp. 46-50.

112. Hammond, C.E., An application of Floquet theory to the prediction of mechanical instability, Journal of the American Helicopter Society, Vol. 19, No. 4, October 1974, pp. 14-23.

113. Bellavita, P., Giorgi, C. and Galeazzi, M., Some aspects of mechanical instability problems for a fully articulated rotor helicopter, Paper No. 14, Proceedings of Second European Rotorcraft and Powered Lift Aircraft Forum, Buckeburg, Germany, September 1976, pp. 14.1-14.40.

114. Hohenemser, K.H., Hingeless rotorcraft flight dynamics, AGARDograph No. 197, September 1974.

115. Bousman, W.G. and Hodges, D.H., An experimental study of coupled rotor-body aeromechanical instability of hingeless rotors in hover, Vertica, Vol. 3, No. 3, 1979, pp. 221-244.

116. Warmbrodt, W. and Friedmann, P., Formulation of coupled rotor/fuselage equations of motion, Vertica, Vol. 3, No. 3, 1979, pp. 254-271.

117. Johnson, W., A comprehensive analytical model of rotorcraft aerodynamics and dynamics, NASA TM 81182, June 1980.

118. Levin, J., Formulation of helicopter air resonance problem in hover with active controls, M.Sc. Thesis, Mechanics and Structures Department, University of California, Los Angeles, September 1981.

119. Greenwood, D.T., Principles of dynamics, Prentice Hall, 1965, p. 51.

120. Warmbrodt, W. and Friedmann, P., Coupled rotor/tower aeroelastic analysis of large horizontal axis wind turbines, AIAA Journal, Vol. 18, No. 9, September 1980, pp. 1118-1124.

121. Bousman, W.G., An experimental investigation of the effects of aeroelastic couplings on the aeromechanical stability of a hingeless rotor helicopter, Journal of the American Helicopter Society, Vol. 26, No. 1, January 1981, pp. 46-54.

122. Johnson, W., The influence of unsteady aerodynamics on hingeless rotor ground resonance, NASA TM 81302, July 1981.

123. Kato, K., Yamane, T., Nagashima, T., Iboshi, N. and Yamagishi, Experimental substantiation for hovering rotor vertical impedance calculations, Journal of Aircraft, Vol. 18, No. 6, June 1981, pp. 445-450.

124. Gaonkar, G.H., Mitra, A.K., Reddy, T.S.R., and Peters, D.A., Sensitivity of helicopter aeromechanical stability to dynamic inflow, Vertica, Vol. 6, No. 1, 1982.

Appendix A: List of Symbols

a = two-dimensional lift curve slope

$\bar{a}$ = acceleration vector, Eq. (3)

$[A]$ = constant matrix, Eq. (20)

$[A(\psi)]^k$ = periodic matrix, Eq. (28)

$\bar{a}_{pk}$ = acceleration vector, for mass point in k^{th} blade, Eq. (33)

A_1, A_2 = coefficients in Wagner function, Eq. (11)

$[B(\psi)]$ = transformation matrix for multiblade coordinates, Eq. (32)

b_1, b_2 = coefficients in the Wagner function Eq. (11)

b = semi-chord

C_L = unsteady lift, coefficient, Eq. (10)

$C(k)$ = Theodorsen's lift deficiency function

$C_{L\alpha}$ = lift curve slope

$C'(k,m,\bar{h}_w)$ = Loewy's lift deficiency function

C_N = unsteady normal force coefficient, in dynamic stall

C_{do} = profile drag coefficient

C_T = thrust coefficient

C_W = $W/\rho_A \pi R^2 (\Omega R)^2$ = weight coefficient

c = airfoil chord

C_{MX} = rolling moment coefficient of rotor

C_{MY} = pitching moment coefficient of rotor

$[C(\psi)]$ = symbolic matric, representing linear damping effects

$[C(\underset{\sim}{X}_o)]$ = linearized damping matrix, for perturbation, equations, Eq. (18)

C_M = unsteady pitching moment coefficient, in dynamic stall

D_P = parasite drag of helicopter, Fig. 17

$\hat{e}_x, \hat{e}_y, \hat{e}_z$ = unit vectors in the directions of the coordinates, x_o, y_o, z_o, respectively before deformation, Figs. 4 and 5

$\hat{e}'_x, \hat{e}'_y, \hat{e}'_z$ = triad $\hat{e}_x, \hat{e}_y, \hat{e}_z$ after deformation, Figs. 4 and 5

e_1 = offset of blade root from axis of rotation, Fig. 4

$\bar{e}_{1z}$ = unit vector in direction of shaft axis, Eq. (34)

$f_k(\psi)$ = generalized coordinate for ϕ degree of freedom, also torsional generalized coordinate of k^{th} blade

$\{f\}^k$ = periodic vector used in quasilinearization, Eq. (28)

Δf_k = perturbation of f_k, Eq. (38)

$\{F_{NL}(\psi, \underset{\sim}{X}, \dot{\underset{\sim}{X}})\}$ = complete nonlinear loading, Eq. (14)

$\{F_{NL}(\psi, q, \dot{q})\}$ = complete nonlinear state vector loading, Eq. (21)

$\{F_{NL}(\underset{\sim}{X}, \dot{\underset{\sim}{X}})\}$ = complete nonlinear loading for hover, Eq. (15)

$\{F_{SN}(\underset{\sim}{X}_o)\}$ = nonlinear loading for static equilibrium in hover, Eq. (17)

g_o = steady state value of g_k, Eq. (38)

$g_i(\psi)$ = generalized coordinate for w degree of freedom

Δg_k = perturbation in flap of k^{th} blade generalized coordinate, Eq. (38)

Δh_k = perturbation in lag of k^{th} blade generalized coordinate, Eq. (38)

h_o = steady state value of h_k, Eq. (38)

h = plunging motion, used in unsteady aerodynamics, Eq. (4)

$h_j(\psi)$ = generalized coordinate for v degree of freedom

$\bar{h}_w$ = (h_w/b) = nondimensional wake spacing

H = inplane force, Fig. 17

[I] = unit matrix

$\underset{\sim}{i}, \underset{\sim}{j}, \underset{\sim}{k}$ = unit vectors in the directions, x,y and z respectively, Fig. 4

i = $\sqrt{-1}$

i,j,k = indices in modal expansion, Eq (13)

k = blade index, in coupled rotor/fuselage formation, Eq. (33)

k = iteration index used in quasilinearization

k = $\omega b/U$ = reduced frequency

$[L(\psi)]$ = linear coefficient matrix, Eq. (21)

L_u = unsteady lift, per unit length, based on Theodorsen theory

L = unsteady lift, per unit length based on Greenberg's theory

ℓ = length of elastic part of the blade

$[L]^{-1}$ = coefficient matrix for dynamic inflow model, Eq. (9)

m = (ω/Ω) = frequency ratio

$[m]$ = coefficient matrix for dynamic inflow model, Eq. (9)

$[M]$ = symbolic inertia (mass) matrix, Eq. (14)

M = Mach number, Fig. 13

M_{pa} = average pitching moment, Fig. 17

N = n_b = number of blades

$\{N(q,\psi)\}$ = nonlinear vector, Eq. (21)

n_F, n_L, n_T = number of global modes used for flap, lag and torsion respectively

P_{HX}, P_{HY} = components of fuselage inertia force in x,y directions respectively

P_{GFX}, P_{GFY} = components of fuselage gravitational force vector

P_{RX}, P_{RY} = components of rotor force vector

P_{GRX}, P_{GRY} = components of the gravitational force vector on rotor

$\bar{P}_{Rk}$ = k^{th} blade force vector, Eq. (36)

$\bar{P}_R$ = total rotor force vector Eq. (36)

$\bar{Q}_R$ = total rotor moment vector, Eq. (36)

Q_{RX}, Q_{RY} = components of rotor moment vector

Q_{HX}, Q_{HY} = components of fuselage inertia moment vector

Q_{GFX}, Q_{GFY} = components of fuselage gravitational moment vector

$\bar{Q}_{Rk}$ = k^{th} blade moment vector, Eq. (36)

$\{q\}$ = unknown state vector, Eq. (21)

$\{q_L\}$ = state vector associated with linear, inhomogeneous system, Eq. (24)

$\{q_H\}$ = state vector associated with linear, homogeneous system, Eq. (25)

$\{\bar{q}(\psi)\}$ = nonlinear periodic equilibrium state about which equations are linearized, Eq. (30)

$\{\Delta q(\psi)\}$ = perturbation of system state, about nonlinear equilibrium position

$\{q_F\},\{q_L\}$ = nodal degrees of freedom for flap and lag bending, respectively, Fig. 16

R_x,R_y,R_z = component of the fuselage mass center displacement vector in the x,y,z directions, respectively

$\bar{r}_{pk}$ = position vector of point in the k^{th} blade in rotating reference frame

$\bar{R}_o$ = position vector of origin of moving coordinate system with respect to inertial reference frame, Eq. (33)

R = blade radius

R_c = elastic coupling parameter

$\bar{R}$ = position vector of a mass point of blade cross section, in blade fixed, rotating reference frame

r = radial station, Fig. 26; Eq. (8)

s = dummy variable, Eq. (26)

[S] = matrix of linear coefficients, for static equilibrium in hover, Eq. (17)

s = 2tU/c = nondimensional time variable in Wagner function, Eq. (11)

[S] = transformation matrix between triads $(\hat{e}_x,\hat{e}_y,\hat{e}_z)$ and $(\hat{e}'_x,\hat{e}'_y,\hat{e}'_z)$, Eq. (1)

t = time

T = thrust

u,v,w = components of the displacement of a point on the elastic axis of the blade in the directions, $\hat{e}_x,\hat{e}_y$ and $\hat{e}_z$, respectively, subscript k, Eq. (37), implies k^{th} blade

U = constant flow velocity in Theodorsen's theory, Eq. (4)

V = pulsating flow velocity in Greenberg's theory, Eq. (5)

V_o = constant part of V

ΔV = varying part of V

V = velocity of forward flight, Fig. 17

v_i = mean induced velocity at the rotor disc

W = weight

x_A = blade cross sectional aerodynamic center (A.C.) offset from elastic axis (E.A.), positive for A C. before E.A.

x_{II} = offset between the elastic axis and tension center of blade cross section, Fig. 5

x_o, y_o, z_o = initial undeformed, blade fixed coordinate system, Fig. 4

$\{X\}$ = generalized coordinate vector, Eq. (14)

x_o = x_o/ℓ = nondimensional coordinate, along elastic part of blade

$\{X_o\}$ = static equilibrium state of $\{X\}$ in hover

$\{\Delta X\}$ = perturbation in $\{X\}$, Eq. (16)

$\{y(\psi)\}$ = perturbed state vector, Eq. (19)

$\{Y\}$ = multiblade coordinate vector, Eq. (32)

$\{Z(\psi)\}$ = known periodic forcing, Eq. (21)

α = airfoil section angle of pitch, Eq. (4)

α_o = constant part of pitch, or angle of attack

$\Delta\alpha$ = harmonically varying part of pitch

α_E = effective angle of attack, Eq. (10)

$\Delta\alpha$ = change in angle of attack for dynamic stall, Eq. (10)

α_R = angle of attack of rotor, Fig. 17

α_{MEAN} = mean angle of attack, Fig. 12

$\Delta\alpha$ = time varying part of angle of attack about α_{MEAN} for dynamic stall, Fig. 12 and 13

$\bar{\alpha}$ = time varying part of angle of attack about α_o for dynamic stall, Fig. 14 and 15

α_W = $\alpha(S) - \alpha_{ES}(S)$ paramter for dynamic stall model

α_S = helicopter shaft angle, Fig. 26

β_p = preconing, inclination of the feathering axis with respect to the hub plane measured in a vertical plane

β_1, β_2 = rigid body flapping angle for teetering rotor, Fig. 3

γ = Lock number

γ_F = flight path angle measured from horizontal, Fig. 17

$\gamma_j(\bar{x}_o)$ = shape functions for v degree of freedom

$\delta\lambda$ = perturbation in steady inflow ratio

ϵ = basis for order of magnitude, associated with typical elastic blade slopes

ε_{QL} = small quantity for quasilinearization convergence test

ζ_k = real part of the k^{th} characteristic exponent

η = real part of characteristic exponent, Figs. 24 and 25

η_{SLi} = viscous structural damping coefficients in percent of critical damping, for the lag modes

η,ζ = cross-sectional coordinates, see Fig. 5

$\eta_i(\bar{x}_o)$ = *shape functions for w degree of freedom*

θ_G = total pitch angle, nonelastic, at pitch bearing about feathering axis

θ_c = critical collective pitch angle, at which linearized system, in hover, becomes unstable

θ_{1s},θ_{1c} = cyclic pitch components

θ = total pitch angle

$\theta_x,\theta_y,\theta_z$ = fuselage rotations, roll, pitch, yaw respectively

λ = inflow ratio

$\bar{\lambda}$ = constant part of the inflow ratio

λ_k = characteristic exponent associated with the k^{th} degree of freedom

$\lambda_o,\lambda_c,\lambda_s$ = components of dynamic inflow perturbation

$\lambda_{1s},\lambda_{1c}$ = cyclic components of inflow ratio

λ = eigenvalue for hover, Eq. (20)

μ = $V\cos\alpha_R/\Omega R$ = advance ratio

ρ_A = density of air

σ_v = $(|\Delta V|/V_o)$ = dimensionless magnitude of the pulsating portion of flow

σ = blade solidity ratio; blade aero/disk area, also damping in Figs. 28-30

ϕ = the rotation of a cross section of the blade around the elastic axis

$\phi_k(\bar{x}_o)$ = shape functions for ϕ degree of freedom, also torsional deflection of k^{th} blade

$\phi(s)$ = Wagner function, corrected for compressibility

$[\phi(\psi)]$ = *transition matrix at time* Ω

$[\phi(2\pi)]$ = transition matrix at end of one period

ψ = azimuth angle of blade ($\psi=\Omega t$) measured from straight aft position

$\bar{\Omega}$ = angular velocity vector, Eq. (3)

ω = frequency

ω_k = imaginary part of the k^{th} characteristic exponent

$\bar{\omega}_{f1}, \bar{\omega}_{L1}, \bar{\omega}_{T1}$ = first rotating natural frequencies in flap, lag and torsion respectively, nondimensionalized w.r.t. Ω

Ω = speed of rotation

$\bar{\omega}_k$ = angular velocity vector, Eq. (34)

$\bar{\omega}_F$ = fuselage angular velocity vector, Eq. (34)

ω_ζ = fundamental rotating lag frequency nondimensionalized w.r.t. Ω

Special Symbols

$(\dot{})$ = differentiation with respect to ψ or t depending on context

$(\ )_{,x}$ = differentiation with respect to x_o

$(\hat{})$ = unit vector

$(\bar{})$ = vector

$\{\ \}, (\underset{\sim}{\ })$ = column matrix

$[\ ]$ = square matrix

$[\ ]^T$ = transpose

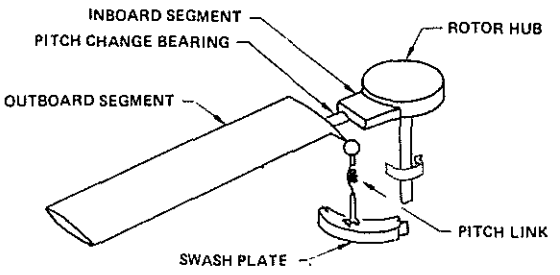

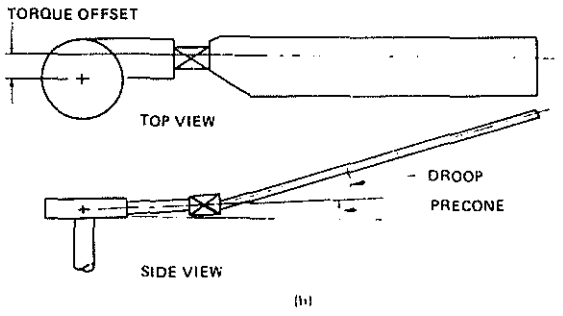

Fig. 1 Typical Hingeless Rotor Configuration

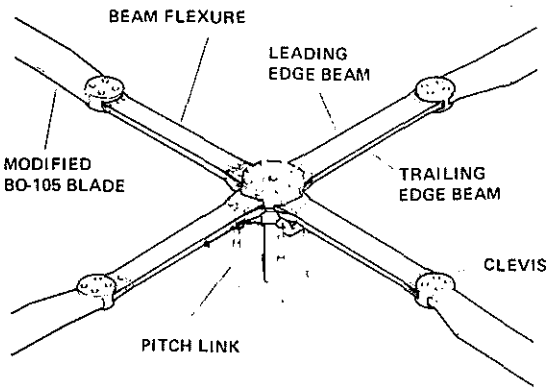

Fig. 2 Bearingless Main Rotor, from Ref. 12

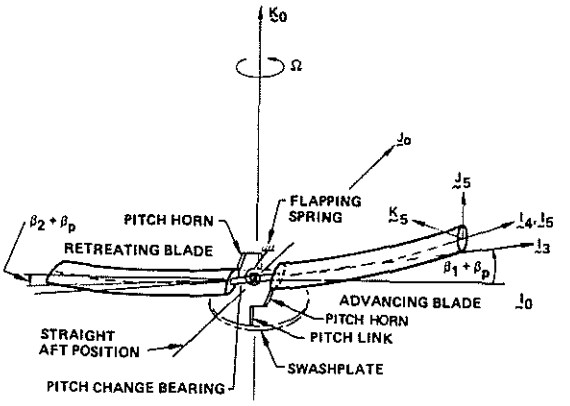

Fig. 3 Typical Geometry for Teetering Rotor Analysis

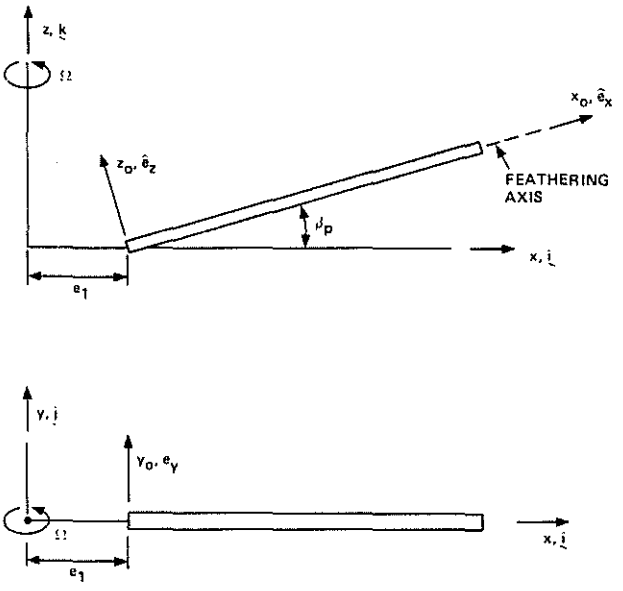

Fig. 4a Typical Description of the Undeformed Blade in the Rotating System x,y,z ($\underset{\sim}{i},\underset{\sim}{j},\underset{\sim}{k}$)

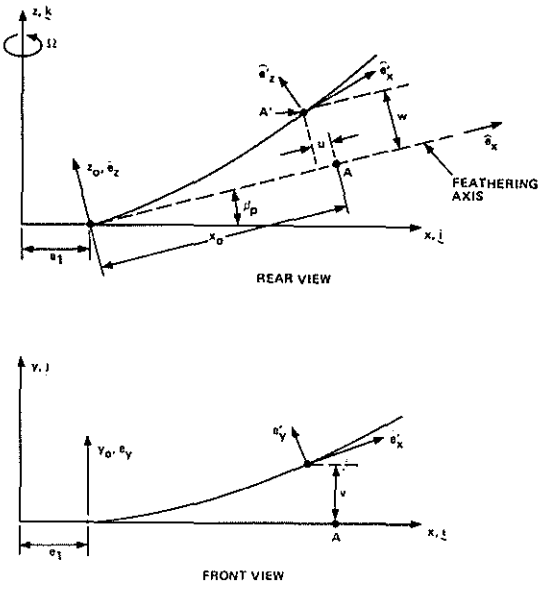

Fig. 4b Geometry of the Elastic Axis of the Deformed Blade

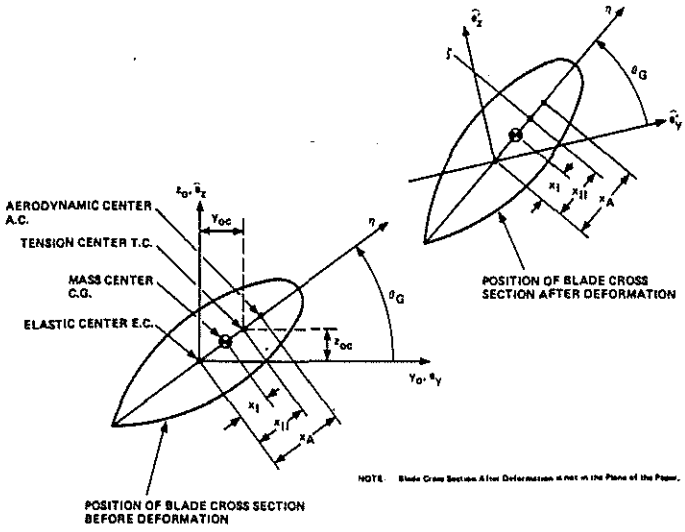

Fig. 5 Blade Cross Section Positions Before and After the Deformation

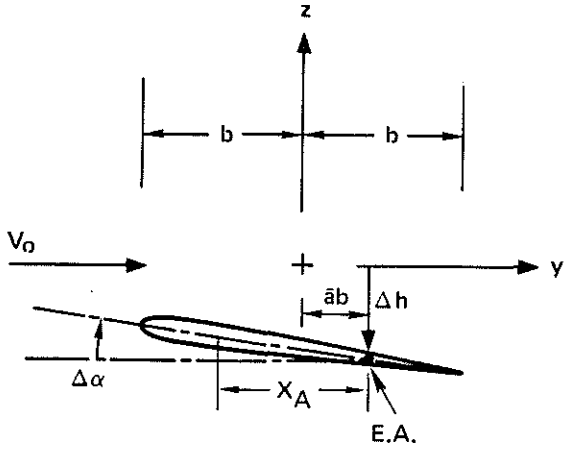

Fig. 6 Geometry of Blade Motion for Conventional Unsteady Aerodynamics

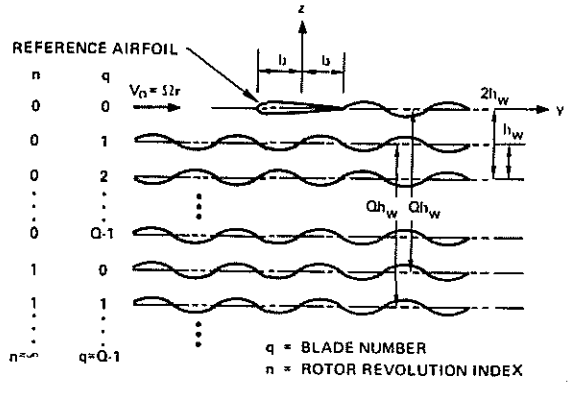

Fig. 7 Geometry for Loewy's Incompressible Unsteady Aerodynamic Model

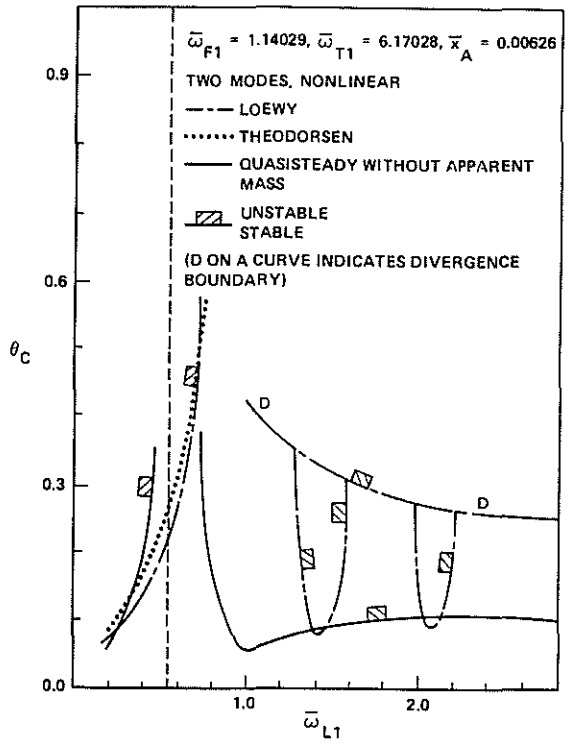

Fig. 8 Effect of Unsteady Aerodynamic Assumptions on Aeroelastic Stability of Hingeless Rotor Blade (based on two modes in each degree of freedom and nonlinear equilibrium position), from Ref. 58

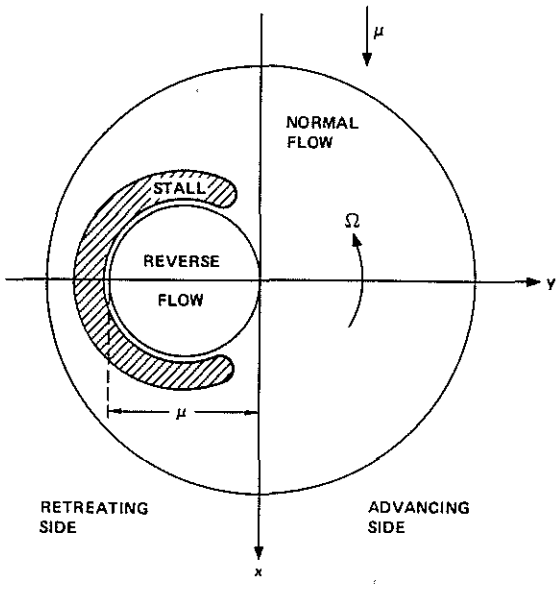

Fig. 9 Schematic Illustration of Reversed Flow and Stall Regions in Forward Flight (μ = 0.70)

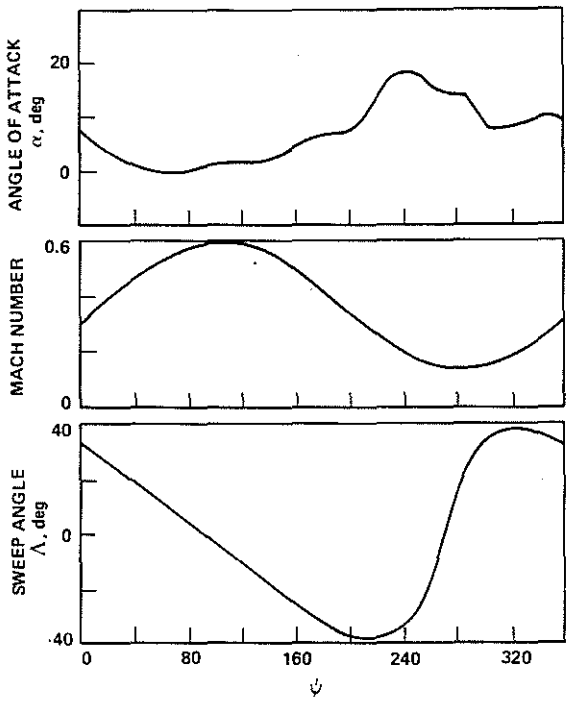

Fig. 10 Typical Blade Section Aerodynamic Properties in Dynamic Stall

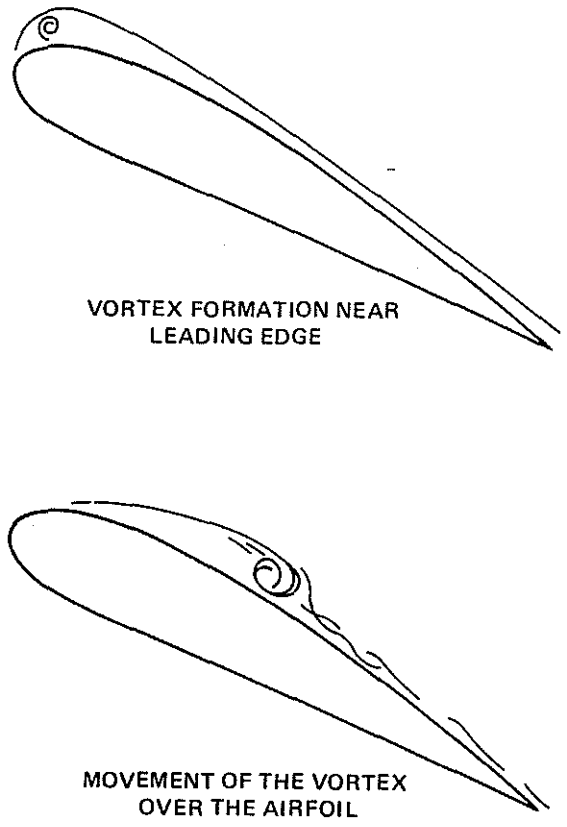

Fig. 11 Vortex Formation and Passage Model Commonly Used in Dynamic Stall Modeling (Ref. 72)

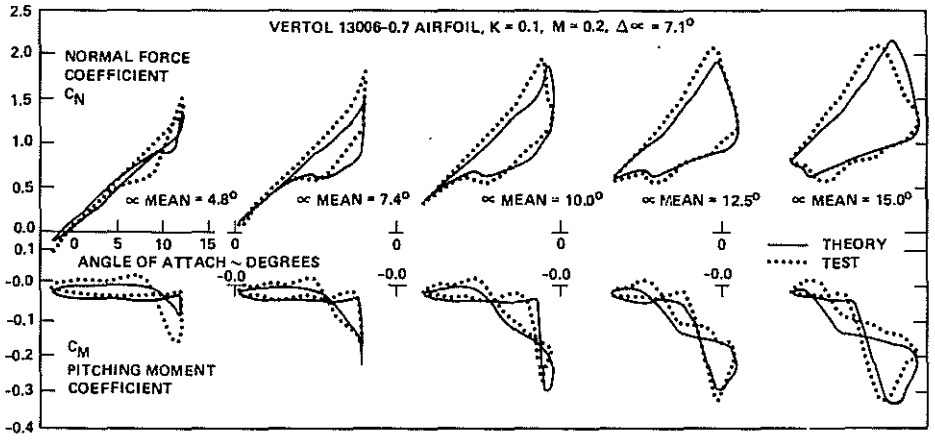

Fig. 12 Effect of Mean Angle of Attack on Synthesized C_N and C_M (Ref. 77)

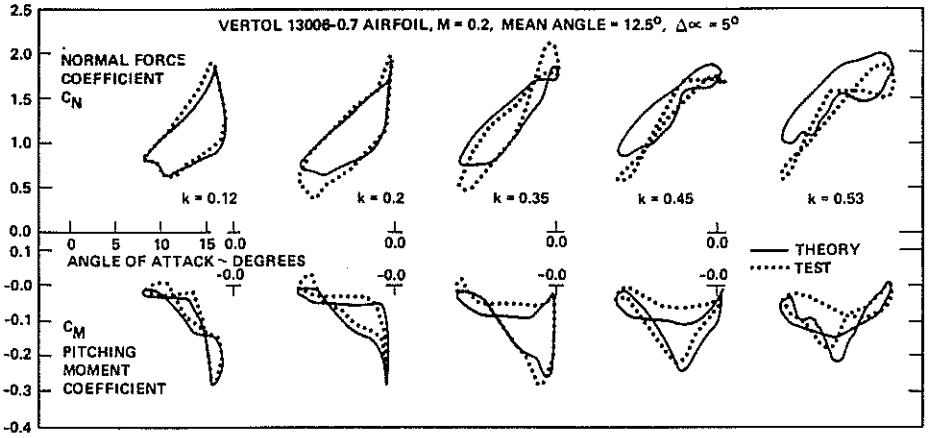

Fig. 13 Effect of Reduced Frequency on Synthesized C_N and C_M (Ref. 77)

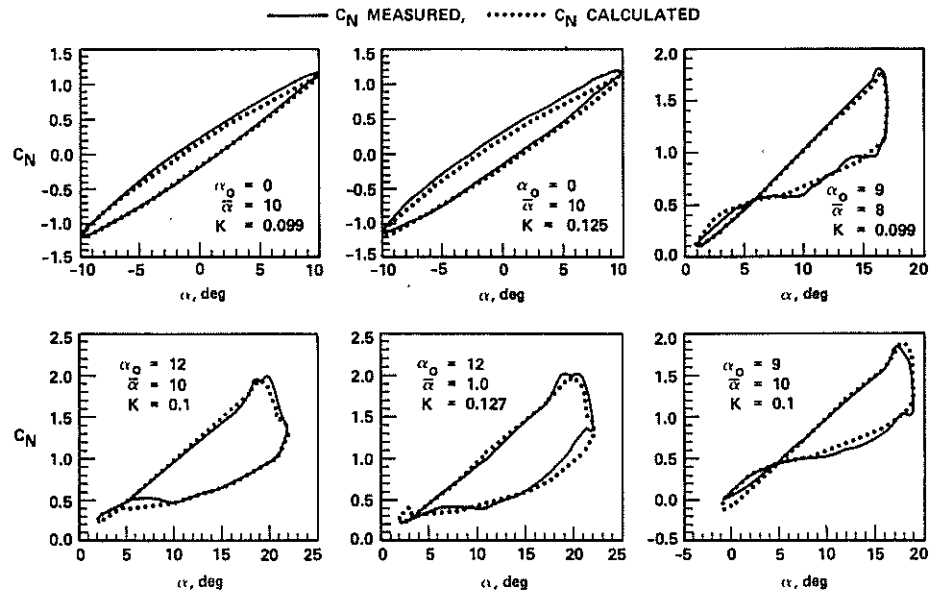

Fig. 14 Comparison of Synthesized C_L (or C_N) Loops with NACA 0012 Test Data at M = 0.30 and Sweep Λ = 0° (Ref. 72)

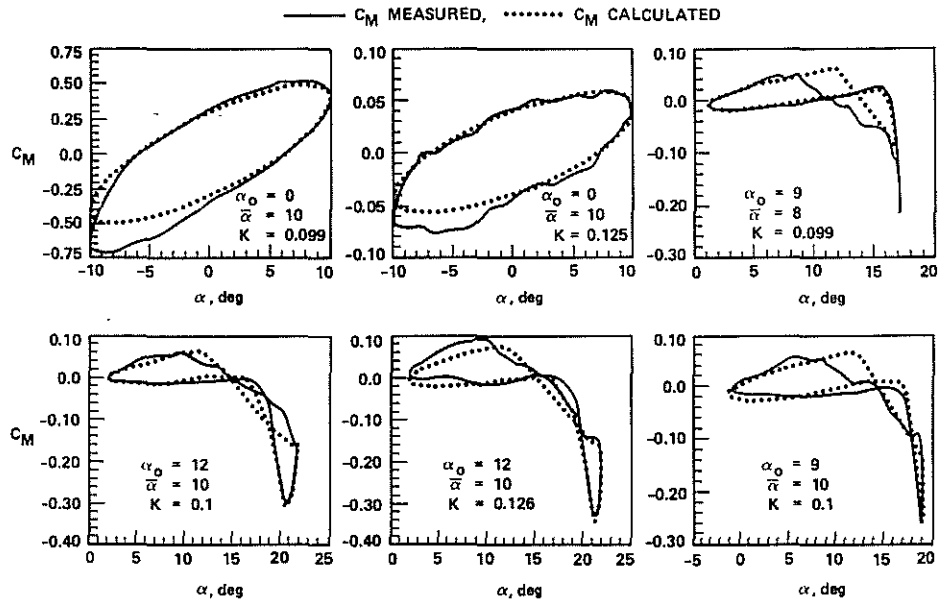

Fig. 15 Comparison of Synthesized C_M Loops with NACA 0012 Test Data at M = 0.30 and Sweep Λ = 0° (Ref. 72)

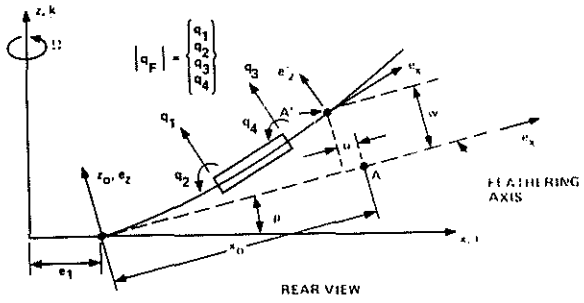

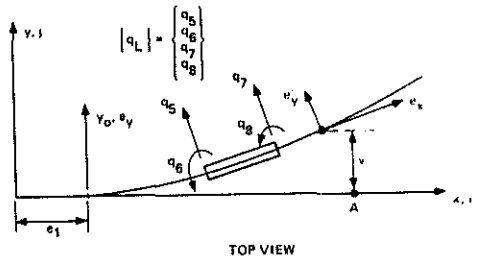

Fig. 16 Geometry of the Elastic Axis of the Deformed Blade and Schematic Representation of the Finite Element Model

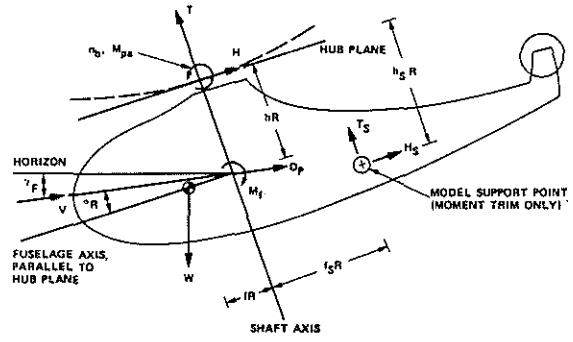

Fig. 17 Longitudinal Forces and Moments for Both Trim Procedures

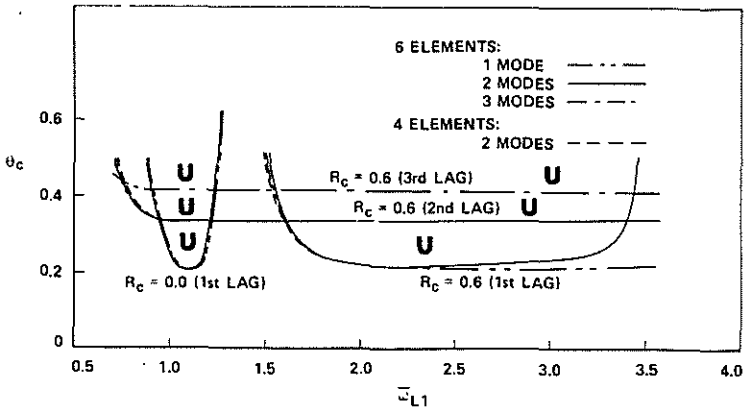

Fig. 18 Convergence of Flap-Lag Stability Boundaries in Hover when the Number of Modes and Elements is Changed (σ = 0.10, γ = 5.0, $\bar{\omega}_{F1}$ = 1.15), Ref. 85

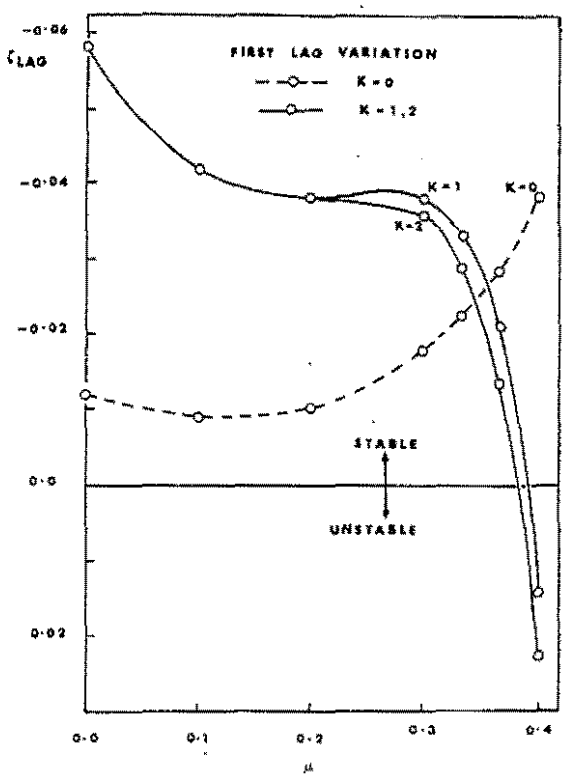

Fig. 19 Stiff-in-Plane Configuration Stability, Propulsive Trim, $C_W = 0.005$ ($\bar{\omega}_{F1} = 1.125$; $\bar{\omega}_{L1} = 1.417$; $\bar{\omega}_{T1} = 3.176$; $\bar{b} = 0.0275$; $\gamma = 5.5$; $a = 2\pi$; $C_{do} = C_{DP} = 0.01$; $n_b = 4$; $\beta_p = 0$; $\sigma = 0.07$), from Ref. 25

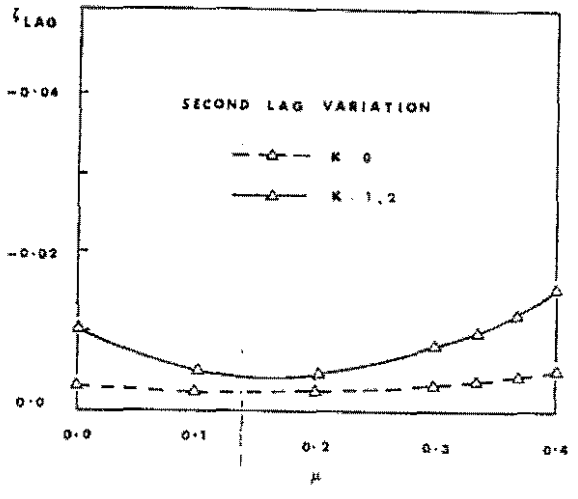

Fig. 20 Stiff-in-Plane Configuration Stability, Same Data as Fig. 19, From Ref. 25

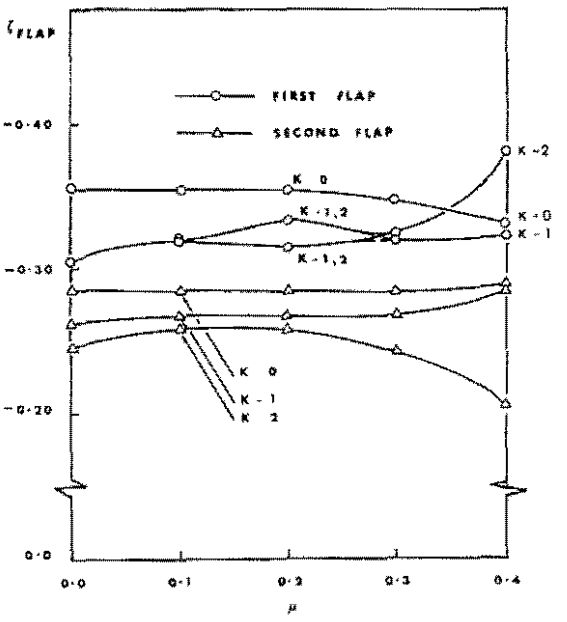

Fig. 21 Stiff-in-Plane Configuration Stability, Same Data as Fig. 19, from Ref. 25

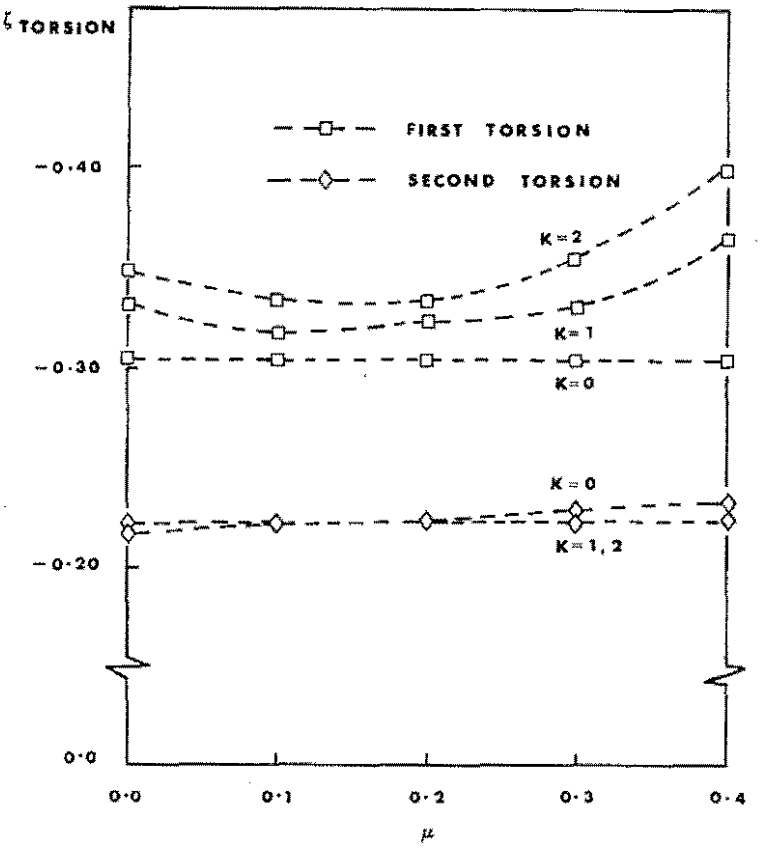

Fig. 22 Stiff-in-Plane Configuration Stability, Same Data as Fig. 19, from Ref. 25

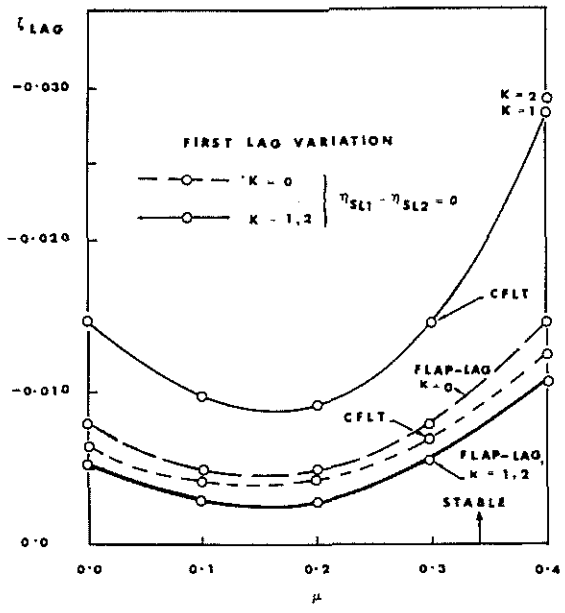

Fig. 23 Blade Stability, Soft-in-Plane Configuration Comparison of Flap-Lag and Coupled Flap-Lag-Torsion Analyses, Propulsive Trim, $C_W = 0.005$, Same Data as Fig. 19 Except $\bar{\omega}_{L1} = 0.732$, from Ref. 25

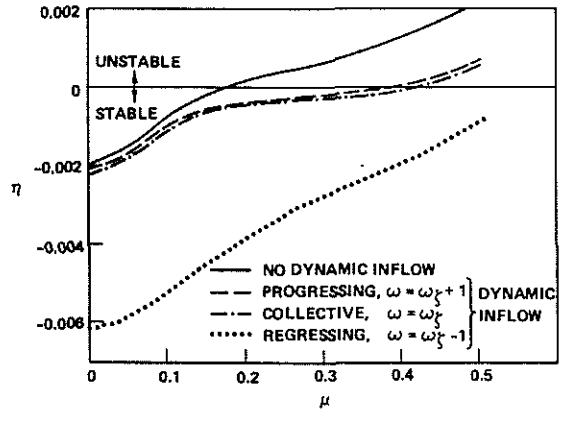

Fig. 24 Effect of Dynamic Inflow on Lead-Lag Mode, $\omega_\zeta = 1.4$, from Ref. 62

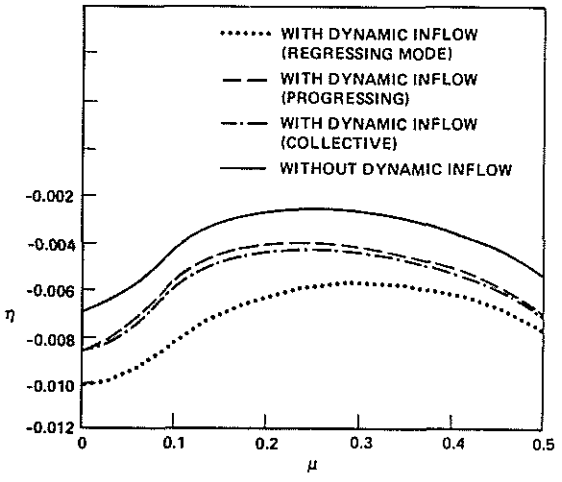

Fig. 25 Effect of Dynamic Inflow on Lead-Lag Mode, $\omega_\zeta = 0.70$, from Ref. 62

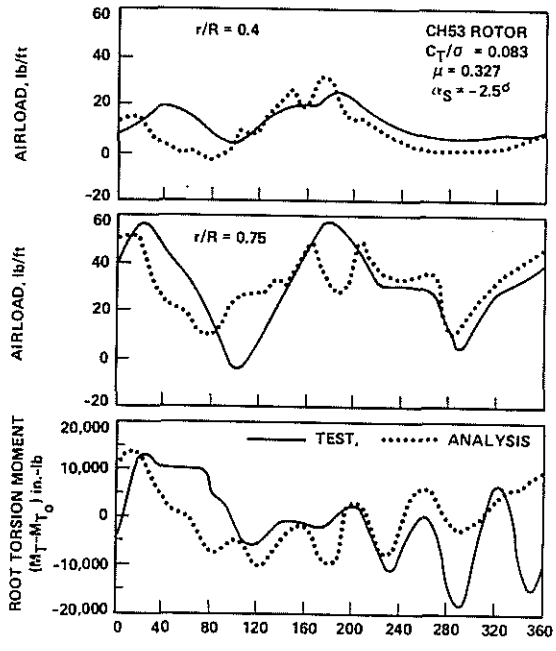

Fig. 26 Correlation Between Calculated and Tested Rotor Blade Airloads and Torsion Moment, from Ref. 72

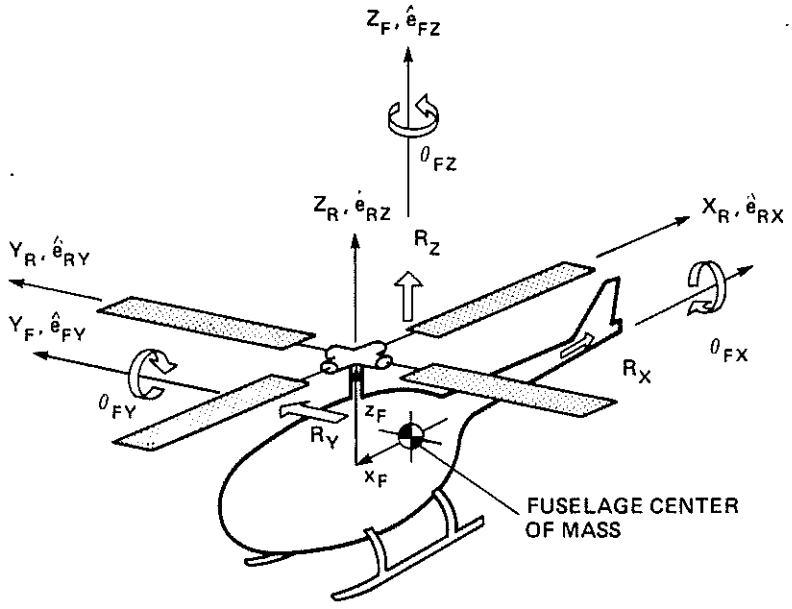

Fig. 27 Rotor/Fuselage Model

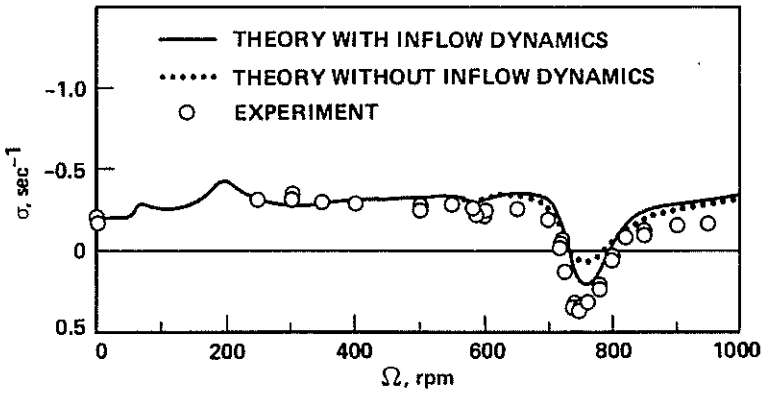

Fig. 28 Regressing Lag Mode Damping as a Function of Rotor Speed, from Ref. 122

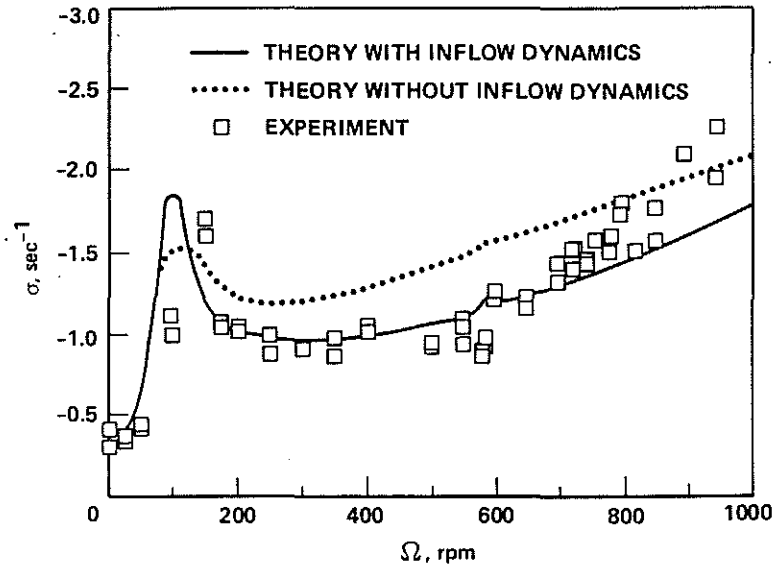

Fig. 29 Body Pitch Mode as a Function of Rotor Speed, from Ref. 122

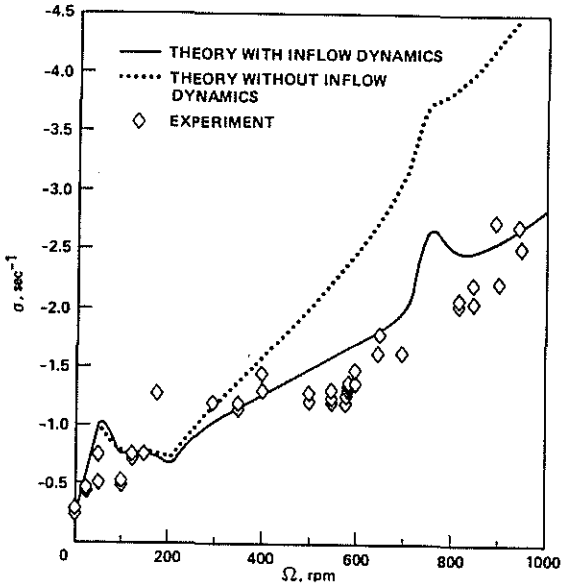

Fig. 30 Body Roll Mode Damping as a Function of Rotor Speed, from Ref. 122